2

The Applications of the Heterodyne Interferoemetry

Cheng-Chih Hsu
Department of Photonics Engineering, Yuan Ze University, Yuan-Tung Road, Chung-Li, Taiwan

1. Introduction

Optical interferometry is widely used in many precision measurements such as displacement[1, 2], vibration[3, 4], surface roughness[5, 6], and optical properties[7-14] of the object. For example, holographic interferomter [1-3] can be used to measure the surface topography of the rigid object. The emulsion side of the photographic plate faces the object and is illuminated by a plane wave at normal incidence. Therefore, the reflection type hologram is recorded the interference signals between the incident wave and scattered wave from the object within the emulsion layer. Then the hologram is reconstructed with laser light and the information of object surface can be obtained. The Speckle interferometry [2-4] can be used to measure the motion of the rough surface. To compare the two exposure specklegrams, then the phase difference related to the surface movement can be obtained. Abbe refractometer [7, 8] is an easy method to determine the refractive index of the material based on the total internal reflection (TIR). That means the refractive index of the testing sample will be limit by the hemisphere prism installed in the refractometer. The ellipsometer [9-12] is widely used to measure the thickness and refractive index of film or bulk materials. Typically, the optical components of ellipsometer included polarizer, compensator, sample, and analyzer. Hence, there were many different types of ellipsometer for refractive index and thickness measurement of the sample. Most popular type is rotating polarizer and analyzer ellipsometer which can be divided into rotating polarizer type and rotating analyzer type. Both of them are analysis of the ellipsometric angles (ψ, Δ) which determined directly from the adjustable angular settings of the optical components. The accuracy of the ellipsometric measurement are typically within the range 0.01° and 0.05° in (ψ, Δ) [13, 14].

Compare to previous method, the heterodyne interferometry give much more flexibility of different kinds of the measurement purposes with suitable optical configuration. In this chapter, I will review the heterodyne interferometry and focus on the applications of this kind of interferometer. First of all, I will briefly introduce the history and applications of heterodyne interferometry that will be discussed in this chapter. Before I mention the applications of the heterodyne interferometry, I would like to describe several types of heterodyne interferometry. Then I would like to describe the precision positioning with optical interferometer and focus on the heterodyne grating interferometer. After that, I will review some refractometer using heterodyne interferometer. In this section I would like to quick look some useful methods for measuring the refractive index and thickness of bulk material or thin film structure. In addition, the measurement of the optic axis and birefringence of the birefringent crystal will also be discussed in this section. The final application of the heterodyne interferometry that I would like to talk about is the concentration measurement. In this section, I will roughly classify the method into two categories. One is fiber type sensor; another is a non-fiber type sensor. And I will discuss the surface plasmon resonance (SPR) sensor in fiber-type and non-fiber type sensors. Finally, I would like to give the short conclusion, which summarized the advantages and disadvantages of the heterodyne interferometer.

2. Heterodyne interferometry

This section will introduce the development history of the heterodyne interferometry and describe the fundamental theory and basic optical configuration of the heterodyne interferometer.

2.1 History of Heterodyne light source developement

Hewlett Packard Company (HP) developed the first commercial heterodyne interferometer for precision positioning since 1966. Until now, HP systems have widely used in industry, scientific research, and education. J. A. Dahlquist, D. G. Peterson, and W. Culshaw [15] demonstrated an optical interferometer, which used Zeeman laser properties in 1966. They had the application of an axial magnetic field and resulted in the frequency difference between the right hand and left hand circular polarization states of the He-Ne laser. Because of these two polarization states are affected by equally thermal drift and mechanism vibration of the laser, the frequency difference are extremely stable. Therefore, this light source with different frequency is so called the heterodyne light source. Figure 1 showed that the first heterodyne interferometer which constructed with Zeeman laser. As you can see, the frequency shift coming from the moving mirror will be carried with ν_2. Then these two lights with different frequency will be interference at 45° and the distance-varying phase can be detected.

There are many methods can construct the optical frequency shift such as rotation or moving grating method [16, 17], accousto-optical modulator (AOM) [18, 19], electro-optical modulator (EOM) [20, 21], and modulating two slightly different wavelengths of laser diodes [22]. Suzuki and Hioki [16] proposed the idea of moving grating method for constructing the heterodyne light source in 1967. As the grating moves along y-axis with the velocity v, the frequency shift will be introduced into the ±1 order diffracted beam with $\pm\frac{v}{a}$. By suitable arrangement of the optical configuration, either one of these frequency shifted signals can be selected and to form the heterodyne light source. W. H. Stevenson [17] proposed the rotation radial grating to form the heterodyne light source in which he showed that the frequency shift were linear increased with the rotation rate of the radial grating up to 6k rpm. And the maximum frequency shift in this case was 500 kHz.

An acousto-optic modulator (AOM) uses the acousto-optic effect to diffract and shift the frequency of the light [18, 19]. The piezoelectric transducer attaches to the quartz and the

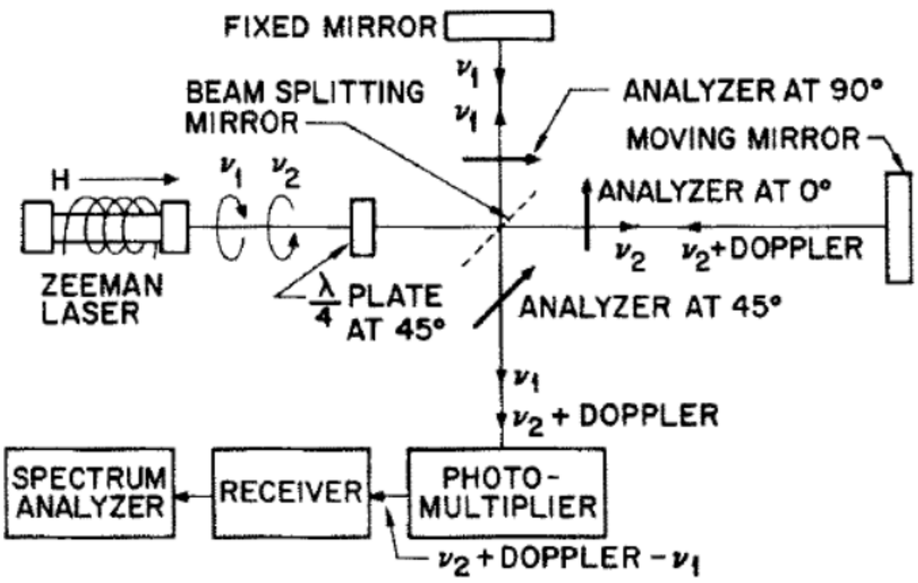

Fig. 1. The first heterodyne interferometer constructed by Zeeman laser [15].

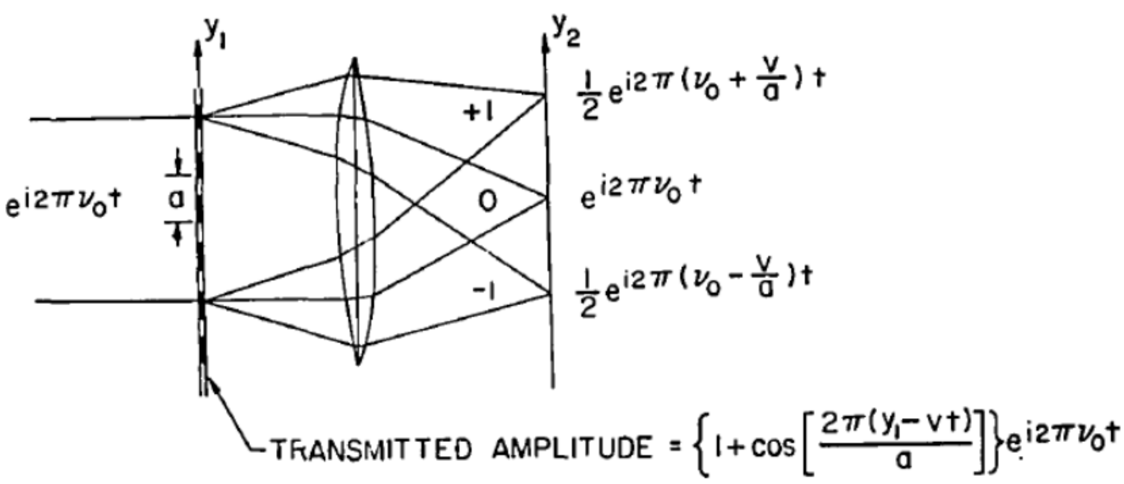

Fig. 2. The heterodyne light source constructed with moving grating [17].

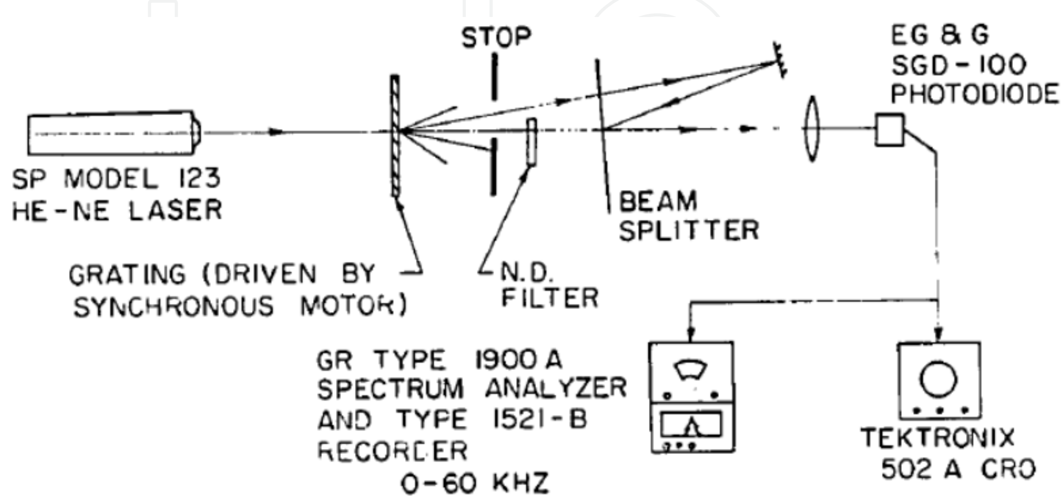

Fig. 3. The heterodyne light source constructed with rotation radial grating [17].

oscillating electric signal drives the transducer to vibrate, which creates sound wave in the quartz and changes the refractive index of the quartz as periodic index modulation. The incoming light diffracts by these moving periodic index modulation planes, which induced the Doppler-shifted by an amount equal to the frequency of the sound wave. That phenomenon is similar to the moving grating method but the fundamental concepts are momentum conservation of the phonon-photon interaction and Bragg diffraction theory. Figure 4 shows the frequency shifted by AOM that proposed in 1988 [18]. A typical frequency shifted varies from 27 MHz to 400 MHz. In the case of M. J. Ehrlich et al. [18], the frequency shifted was 29.7 MHz and the induced phase shifted over 360° by applying the voltage within 15 V.

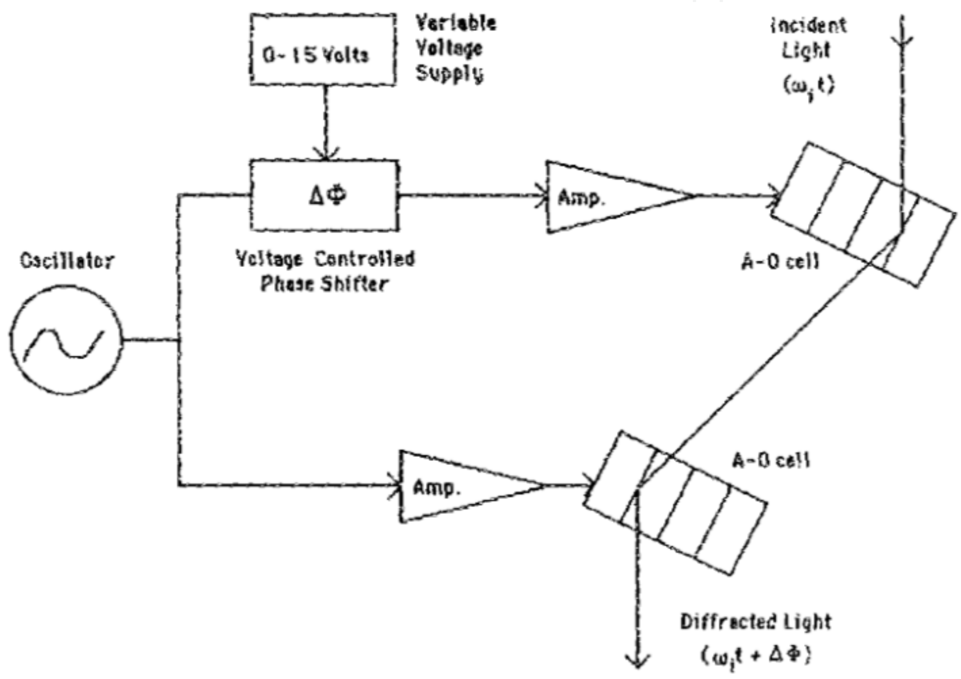

Fig. 4. The frequency shifted by AOM [18].

Electro-optic modulator is a signal-controlled optical device that based on the electro-optic effect to modulate a beam of light. The modulation may be imposed the phase, amplitude, or frequency of the modulated beam. Lithium niobate ($LiNbO_3$) is one of the electro-optic crystals that is widely used for integrated optics device because of its large-valued Pockels coefficients. The refractive index of $LiNbO_3$ is a linear function of the strength of the applied electric field, which is called Pockel effect. Figure 5 shows one of the optical configurations of the heterodyne light source constructed by EOM. The linear polarized light into the EOM, which the crystal axis is located at 45° respected to the x-axis and applied half-wave voltage $V_{\lambda/2}$ on it, the outcome light will carry the frequency shifted.

The wavelength of laser diode can be varied as the injection current and temperature of the laser diode. The wavelength increased as the injection current increased. In general, the rate of the increase is about 0.005 nm/mA at 800 nm and that will be different for different types of laser diode [22]. As the wavelength of the laser diode is changed from λ to $\lambda+\Delta\lambda$ periodically, in which the injection current is periodically changed, the frequency shift of the heterodyne signal can be obtained.

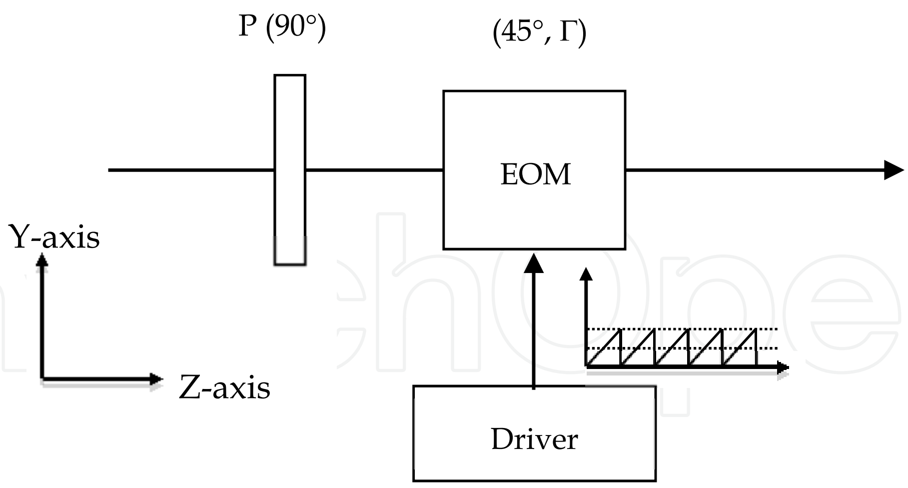

Fig. 5. The optical setup of heterodyne light source with EOM.

2.2 Type of Heterodyne interferometer

The heterodyne interferometer can be divided into two categories, one is common-path type and another is non common-path type. The common-path means that the environment influence of the polarization states of the interference signal can be ignored. Of course, one also can divide into linear polarized heterodyne and circular polarized heterodyne interferometers based on the heterodyne light source. In this section, we would like to describe that based on heterodyne light source and focus on the boundary phenomena between the heterodyne light source and testing sample.

The optical configuration of the linear polarized heterodyne light source have described in figure 5. For convenient, assume that the light propagate along z-axis and vertical direction is y-axis. If the fast axis of the EOM is located at 45° respected to the x-axis, the Jones matrix can be described [14, 23]:

$$\mathrm{EO}(45°,\Gamma) = \begin{pmatrix} \cos 45^o & -\sin 45^o \\ \sin 45^o & \cos 45^o \end{pmatrix} \begin{pmatrix} e^{i\frac{\Gamma}{2}} & 0 \\ 0 & e^{-i\frac{\Gamma}{2}} \end{pmatrix} \begin{pmatrix} \cos 45^o & \sin 45^o \\ -\sin 45^o & \cos 45^o \end{pmatrix} = \begin{pmatrix} cos\frac{\Gamma}{2} & i\,sin\frac{\Gamma}{2} \\ i\,sin\frac{\Gamma}{2} & cos\frac{\Gamma}{2} \end{pmatrix} \tag{1}$$

where the Γ is the phase retardation of EOM and can be described $\Gamma = \frac{\pi V}{V_{\lambda/2}}$. When we applied half-wave voltage of the EOM with sawtooth electric signal, equation (1) can be approximated as

$$\mathrm{EO}(\omega t) = \begin{pmatrix} e^{-im\pi\frac{i\omega t}{2}} & 0 \\ 0 & e^{im\pi\frac{-i\omega t}{2}} \end{pmatrix} = \begin{pmatrix} e^{i\frac{\omega t}{2}} & 0 \\ 0 & e^{-i\frac{\omega t}{2}} \end{pmatrix} \tag{2}$$

As a linear polarized light with the polarization direction at 45° pass through the EOM, then the E-field can be

$$E = EO(\omega t) \cdot E_{in} = \begin{pmatrix} e^{i\frac{\omega t}{2}} & 0 \\ 0 & e^{-i\frac{\omega t}{2}} \end{pmatrix} \cdot \frac{1}{\sqrt{2}} \binom{1}{1} e^{i\omega_0 t} = \frac{1}{\sqrt{2}} \begin{pmatrix} e^{i\frac{\omega t}{2}} \\ e^{-i\frac{\omega t}{2}} \end{pmatrix} e^{i\omega_0 t} \tag{3}$$

where ω_0 and ω are optical frequency and frequency shifted between two orthogonal polarization state, respectively. Obviously, equation (3) described the linear polarized heterodyne light source.

For a circular polarized heterodyne light source, the optical configuration is showed in figure 6. As a linear polarized light pass through EOM and quarter-wave plate Q with the azimuth angle at 0°, the Jones matrix of the E-field of the outcome light can be described

$$E' = Q(0°)\cdot EO(\omega t)\cdot E_{in}$$
$$= \begin{pmatrix}1 & 0\\ 0 & i\end{pmatrix}\begin{pmatrix}\cos(\omega t/2) & i\sin(\omega t/2)\\ i\sin(\omega t/2) & \cos(\omega t/2)\end{pmatrix}\begin{pmatrix}1\\0\end{pmatrix} = \begin{pmatrix}\cos(\omega t/2)\\ -\sin(\omega t/2)\end{pmatrix}$$
$$= \frac{1}{2}\begin{pmatrix}1\\ i\end{pmatrix}e^{\frac{i\omega t}{2}} + \frac{1}{2}\begin{pmatrix}1\\ -i\end{pmatrix}e^{-\frac{i\omega t}{2}}. \tag{4}$$

Obviously, equation (4) describes the circular heterodyne light source that indicated the frequency shifted ω between left-hand circular polarized light and right-hand circular polarized.

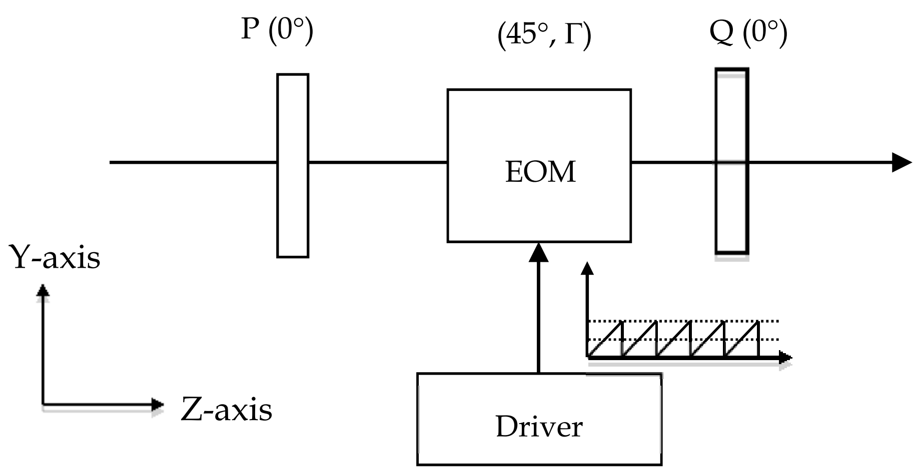

Fig. 6. The circular polarized heterodyne light source.

If the optical interferometer is constructed of the circular polarized heterodyne light source, we always call that circular heterodyne interferometer otherwise we call that heterodyne interferometer. For the specific purpose, we will arrange the tested system as transmission type, reflection type, and multi-reflection type according to the optical property of the testing sample. These types are summarized and show in figure 7. It is obvious that the polarization states (p- and s- polarization states or right-hand and left-hand circular polarization states) of the heterodyne light source are propagated at the same optical path, in which we call common-path structure. The advantage of the common-path structure is the influence of the polarization states of the heterodyne light source can be assumed and limited to the acceptable value. In general, we can ignore the error when the measurement system with common-path configuration. In figure 7, the reference signal I_r coming from the function generator can be written as

$$I_r = I'[1+\cos(\omega t)], \tag{5}$$

and direct into the lock-in amplifier. The heterodyne light source will pass through or reflect from the tested system and then pass through the analyzer AN_t with azimuth angle at α, finally detect by photodetector D_t. The tested system can be divided into three types based on the optical property of the testing sample. There are transmission, reflection, and multi-reflection types.

To consider a heterodyne light source passed through the transmission materials which induced the phase retardation φ, the E-field and intensity detected by D_t can be written as

$$E_t = AN_t(\alpha) \cdot W \cdot E_{in} = \frac{1}{2}\begin{pmatrix} 1 & 1 \\ 1 & 1 \end{pmatrix}\begin{pmatrix} e^{\frac{i\varphi}{2}} & 0 \\ 0 & e^{-\frac{i\varphi}{2}} \end{pmatrix}\begin{pmatrix} \cos\frac{\omega t}{2} \\ -\sin\frac{\omega t}{2} \end{pmatrix},$$

$$= [\cos\alpha\cos\frac{\omega t}{2}e^{i\frac{\varphi}{2}} - \sin\alpha\sin\frac{\omega t}{2}e^{-i\frac{\varphi}{2}}] \cdot \begin{pmatrix} \cos\alpha \\ \sin\alpha \end{pmatrix} \tag{6}$$

and

$$I_t = |E_t|^2 = \frac{1}{2}\left[1 + 2\sqrt{A^2 + B^2}\cos(\omega t + \phi)\right] \tag{7}$$

where W is the Jones matrix of testing sample at transmission condition; A, B, and ϕ can be written as

$$A = \frac{1}{2}(\cos^2\alpha - \sin^2\alpha), \tag{8a}$$

$$B = \cos\alpha\sin\alpha\cos\varphi, \tag{8b}$$

and

$$\phi = \tan^{-1}(\frac{B}{A}) = \tan^{-1}\frac{2\cos\alpha\sin\alpha\cos\varphi}{(\cos^2\alpha - \sin^2\alpha)}, \tag{8c}$$

It is obvious that the phase retardation φ will be carried by the testing signal I_t. To compare I_r and I_t with lock-in amplifier, the phase difference ϕ coming from the testing sample can be obtained. Substitute the phase difference into equation (8c), the phase retardation of the sample can be determined.

Of course, if the testing sample is not transparence, the reflection type or multi-reflection type can be applied to measure the optical property of the testing sample. To consider a circular heterodyne light source is reflected by the testing sample, passed through the analyzer with the azimuth angle α, and finally detected by photodetector. According to Jones calculation, the E-field and intensity can be expressed as

$$E_t = AN(\alpha) \cdot S \cdot E'$$

$$= \begin{pmatrix} \cos^2\alpha & \sin\alpha\cos\alpha \\ \sin\alpha\cos\alpha & \sin^2\alpha \end{pmatrix}\begin{pmatrix} r_p & 0 \\ 0 & r_s \end{pmatrix}\begin{pmatrix} \cos\frac{\omega t}{2} \\ -\sin\frac{\omega t}{2} \end{pmatrix}$$

$$= \left(r_p\cos\alpha\cos\frac{\omega t}{2} - r_s\sin\alpha\sin\frac{\omega t}{2}\right)\begin{pmatrix} \cos\alpha \\ \sin\alpha \end{pmatrix} \tag{9}$$

and

$$I_t = |E_t|^2 = I_0[1 + \cos(\omega t + \phi)] \quad . \tag{10}$$

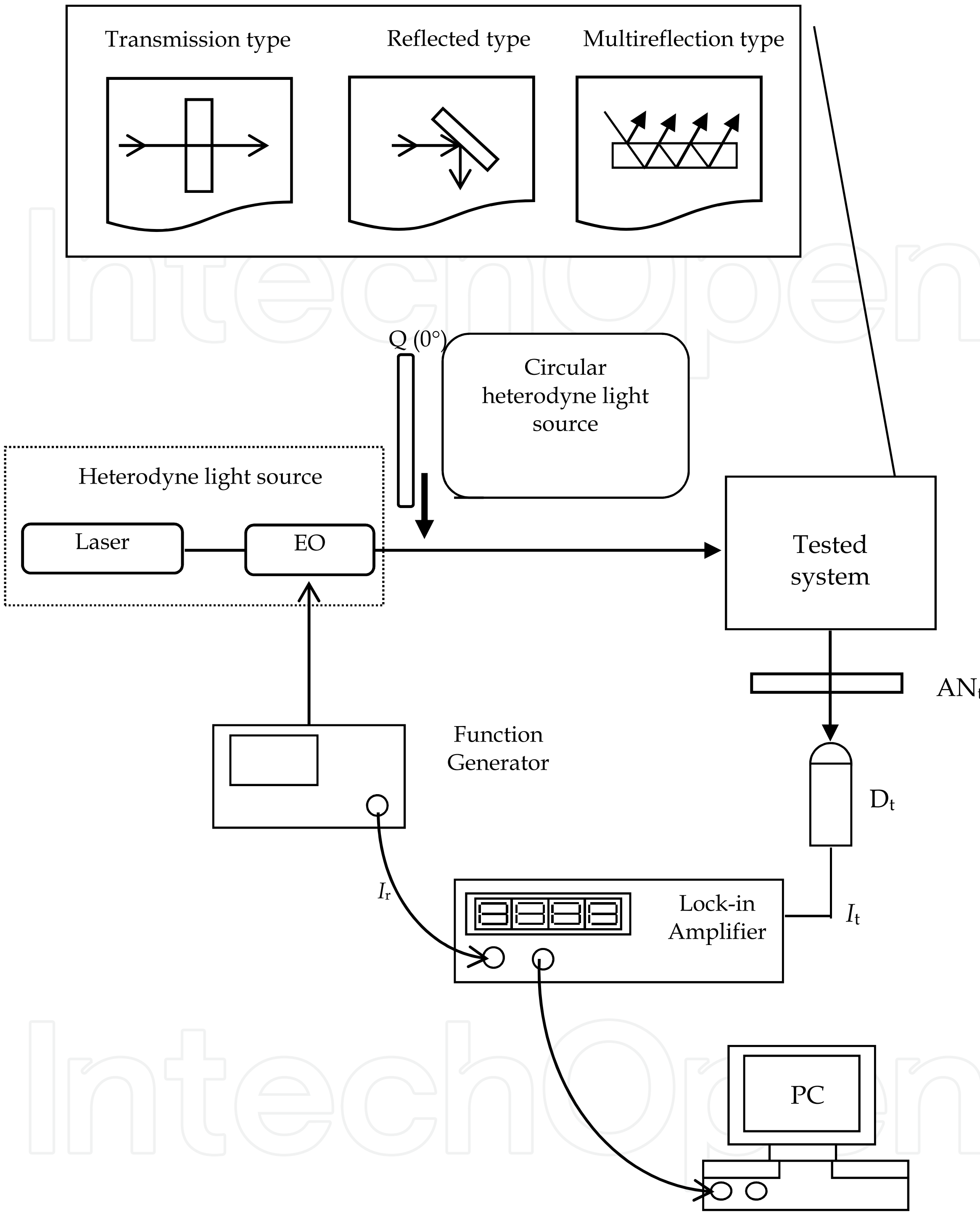

Fig. 7. Types of the heterodyne interferometer with common-path structure.

Where **S** is the Jones matrix of testing sample at reflection condition, r_p and r_s are the reflection coefficients, I_0 and ϕ are the average intensity and phase difference coming from the sample between p- and s- polarizations, which can be written as

$$I_0 = \frac{(r_p{}^2 \cos^2 \alpha + r_s{}^2 \sin^2 \alpha)}{2} \tag{11a}$$

and

$$\phi = \tan^{-1}\left(\frac{2\sin\alpha\cos\alpha\cdot r_p r_s}{r_p{}^2\cos^2\alpha + r_s{}^2\sin^2\alpha}\right) \tag{11b}$$

The reflection coefficients in the reflection matrix of the sample can be expressed by Fresnel equation that can be divided into single reflection and multi-reflection depended on the testing structure. Hence, the r_p and r_s can be written as [14, 23]

(1) single reflection

$$r_p = \frac{n_2\cos\theta - n_1\cos\theta_t}{n_2\cos\theta + n_1\cos\theta_t}, \tag{12a}$$

$$r_s = \frac{n_1\cos\theta - n_2\cos\theta_t}{n_1\cos\theta + n_2\cos\theta_t}, \tag{12b}$$

(2) multi-reflection

$$r_p(\beta) = \frac{r_{1p} + r_{2p}\exp(i\beta)}{1 + r_{1p}r_{2p}\exp(i\beta)}, \tag{13a}$$

$$r_s(\beta) = \frac{r_{1s} + r_{2s}\exp(i\beta)}{1 + r_{1s}r_{2s}\exp(i\beta)}, \tag{13b}$$

and

$$\beta = \frac{2\pi n_2 d\cos(\theta_t)}{\lambda}. \tag{13c}$$

Where n_1 and n_2 are the refractive indices of air and testing sample, θ and θ_t are the incident angle and refracted angle, β is the phase difference coming from the optical path difference in the testing sample, λ is the wavelength of the heterodyne light source. It is obvious that the optical properties of the testing sample can be obtained by substitute phase difference into the equations (10) ~ (13).

On the other hand, the typical optical configuration of the non-common path is shown in figure 8. It is clear that p- and s- polarizations will be propagated at two different paths when they passed through the polarization beam splitter (PBS). In practice, the environment disturbance will not be neglected in non-common path configuration because of these two orthogonal polarization states will have different influence at different path. Therefore, the non-common path optical interferometry using for precision measurement should be seriously taken consideration of stability of the environment disturbance. Figure 8 shows the optical configuration of the displacement measurement. The p- and s- polarizations will reflect by mirrors M_1 and M_2, then pass through the analyzer with azimuth angle at 45°. Therefore, the E-field and intensity of the interference signal between two arms can be written as

$$E_t = \begin{pmatrix} e^{\frac{i\omega t}{2} - ik(2d_p)} \\ e^{\frac{i\omega t}{2} - ik(2d_s)} \end{pmatrix} e^{i\omega_0 t}, \tag{14}$$

and

$$I_t = \frac{1}{2}\left\{1 + \cos\left[\omega t - \frac{4\pi}{\lambda}(d_p - d_s)\right]\right\}. \tag{15}$$

If the mirror M_1 is moved with time, the phase difference $\frac{4\pi d_p}{\lambda}$ will be changed and the displacement variation can be measured by comparing the testing signal and reference signal with lock-in amplifier.

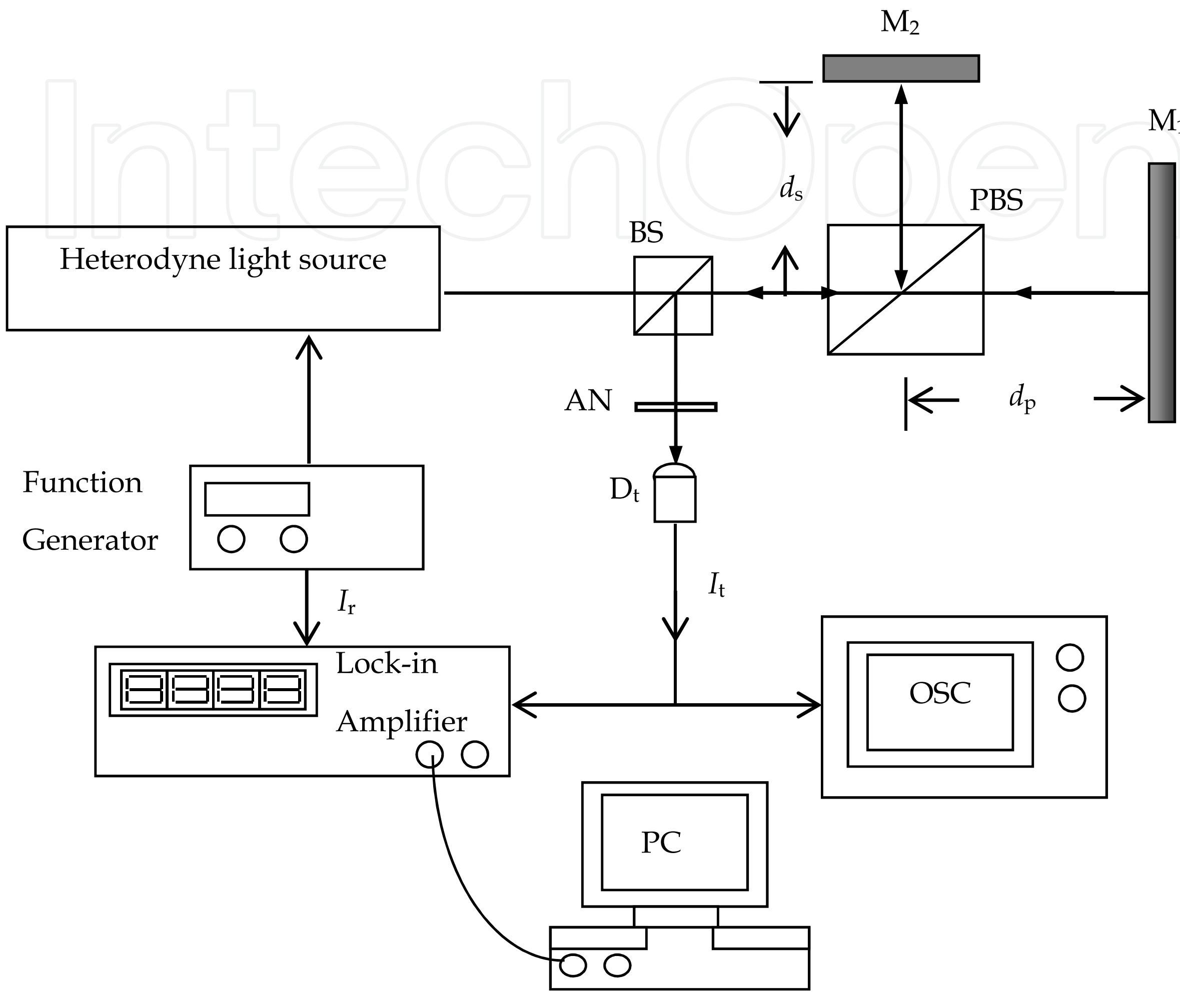

Fig. 8. The optical configuration of the non-common path displacement measurement.

3. Accurate positioning with heterodyne interferometer

Nano-scale positioning devices have become a significant requirement in scientific instruments used for nanotechnology applications. These devices can be applied to nano-handling, nanomanipulation, and nanofabrication. In addition, they are an essential part of the scanning probe microscopy (SPM) and widely used in many research fields. The precision positioning devices consist of three principle parts, which are the rolling component, the driving system and the position sensor. Piezoelectric actuator is the most popular method for driving system and commercial products have been on the market for a few decades. Therefore, the piezoelectric actuator and the position sensor will play the role of the positioning and the feedback control of the rolling element. To achieve the high resolution positioning, the sensing methods of position sensor become more important and have attracted great attention over the past two decades. In this section, we will introduce a few of typical precision positioning methods [24-30] which used heterodyne interferometry.

C. C. Hsu [29] proposed the grating heterodyne interferometry (GHI) to measure the in-plane displacement. The schematic diagram of this method is shown in figure 10. The diffracted grating has mounted on the motorized stage and four diffracted lights will diffract and propagate in the x-z and y-z planes which are for measuring the displacement in x- and y- directions respectively. Based on the Jones calculation, the E-field of the ±1 diffracted beams can be expressed

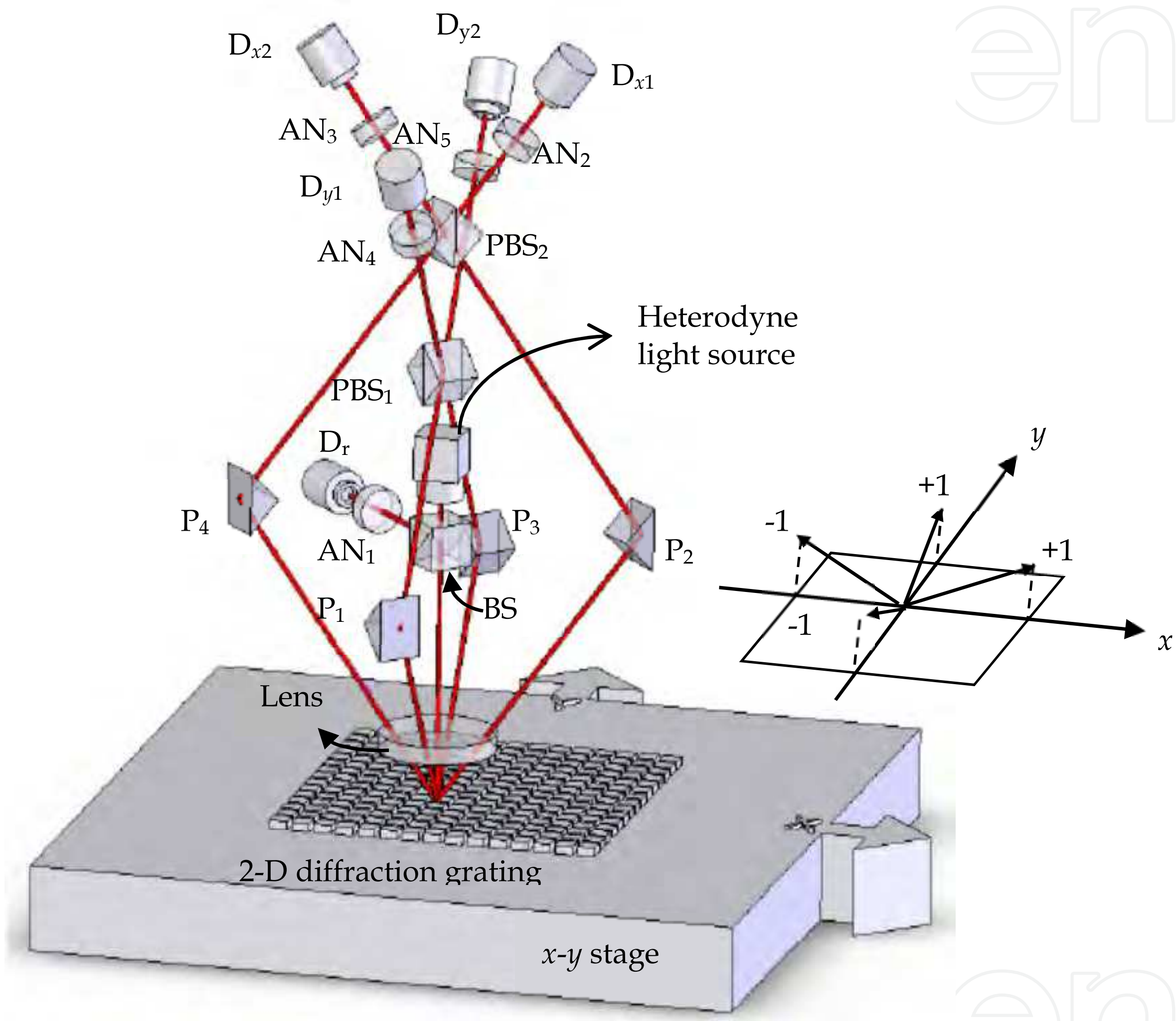

Fig. 10. 2-D displacement measurement system with GHI [29].

$$E_{x\pm1} \propto \exp\left(ikl_{x\pm1} \pm i\frac{2\pi}{g_x}d_x\right)\cdot E_H = \exp\left(ikl_{x\pm1} \pm i\frac{2\pi}{g_x}d_x\right)\begin{pmatrix} e^{i\omega t/2} \\ e^{-i\omega t/2}\end{pmatrix}, \text{(x-direction)} \quad (16a)$$

and

$$E_{y\pm1} \propto \exp\left(ikl_{y\pm1} \pm i\frac{2\pi}{g_y}d_y\right)\cdot E_H = \exp\left(ikl_{y\pm1} \pm i\frac{2\pi}{g_y}d_y\right)\begin{pmatrix} e^{i\omega t/2} \\ e^{-i\omega t/2}\end{pmatrix}, \text{(y-direction)} \quad (16b)$$

where g_x and g_y are the grating pitch in x- and y- directions, d_x and d_y are the displacement along the x- and y- directions respectively. To consider x-direction displacement measurement, the ±1st order diffracted lights will be collected by a lens L and propagate into two paths: (1) prism P_2 → polarization beam splitter PBS_2 → analyzer AN_2 (45°) → detector

D_{x1}, (2) prism $P_4 \rightarrow$ polarization beam splitter $PBS_2 \rightarrow$ analyzer AN_3 (45°) $\rightarrow$ detector D_{x2}. It is similar to the y-direction displacement measurement, the ±1st order diffracted lights will be propagated into (3) prism $P_1 \rightarrow$ polarization beam splitter $PBS_2 \rightarrow$ analyzer AN_4 (45°) $\rightarrow$ detector D_{y1}, (4) prism $P_3 \rightarrow$ polarization beam splitter $PBS_2 \rightarrow$ analyzer AN_5 (45°) $\rightarrow$ detector D_{y2}. After Jones calculation, they can be written as

$$I_{x1} \propto \left|E_{+1s,x} + E_{+1p,x}\right|^2 = \frac{1}{2}\left[1 + \cos\left(\omega t + k\left(l_{-1,x} - l_{+1,x}\right) - \frac{4\pi}{g_x} d_x\right)\right], \tag{17a}$$

$$I_{x2} \propto \left|E_{-1s,x} + E_{+1p,x}\right|^2 = \frac{1}{2}\left[1 + \cos\left(\omega t + k\left(l_{+1,x} - l_{-1,x}\right) - \frac{4\pi}{g_x} d_x\right)\right], \tag{17b}$$

$$I_{y1} \propto \left|E_{+1s,y} + E_{-1p,y}\right|^2 = \frac{1}{2}\left[1 + \cos\left(\omega t + k\left(l_{-1,y} - l_{+1,y}\right) - \frac{4\pi}{g_y} d_y\right)\right], \tag{18a}$$

and

$$I_{y2} \propto \left|E_{-1s,y} + E_{+1p,y}\right|^2 = \frac{1}{2}\left[1 + \cos\left(\omega t + k\left(l_{+1,y} - l_{-1,y}\right) - \frac{4\pi}{g_y} d_y\right)\right]. \tag{18b}$$

To compare the equations (17) and (18), the phase difference coming from the movement in x- and y- directions can be obtained and expressed as

$$\phi_i = \frac{8\pi}{g_i} d_i + 2kl_i \quad (i = x, y), \tag{19}$$

where l_x and l_y are the path difference between grating and PBS_1 and PBS_2 respectively. In practice, the second term in equation (19) can be assumed the initial phase. Therefore, the displacement can be obtained as phase difference is measured and grating pitch is given.

Figure 11 shows that the 2-D displacement measurement with 2-D grating. The movement of the stage is toward to 45° respected to the x-direction and moved 180 nm. The displacement projection in the x- and y-direction are about 120 nm and 140 nm respectively. It is obvious that there are small difference between the results measured by GHI and HP 5529A. Hsu's results can observe that the sensitivity of GHI is higher than HP 5529A and the smallest displacement variation can be judged is about 6 pm. Besides, GHI can provide the 2-D displacement monitoring with single measurement apparatus which have many advantages such as easy alignment, high cost/preference ratio, and easy integrated to the motorized system.

Recently, J. Y. Lee [30] proposed a novel method to measure the 2-D displacement which have quasi-common optical path (QCOP) configuration. The optical structure is shown in figure 12. Based on the clever arrangement, the expanded heterodyne beam is divided into 4 parts *A*, *B*, *C* and *D*. According to the Jones calculation, the amplitudes of these 4 parts are given by

$$E_B = E_C = J(180°) \cdot E_H = \begin{pmatrix} e^{-i\omega t/2} \\ e^{i\omega t/2} \end{pmatrix}, E_A = E_D = J(0°) \cdot E_H = \begin{pmatrix} e^{i\omega t/2} \\ e^{-i\omega t/2} \end{pmatrix}. \tag{20}$$

The expanded heterodyne beam will reflect by a mirror and focus by a lens with suitable focal length, in which can make the zero order (m=0) beam overlap with the ±1 order diffracted beams. The beam distribution is shown in detail in the inset. When the grating moves along the x direction, the interference phase changes can be observed from the

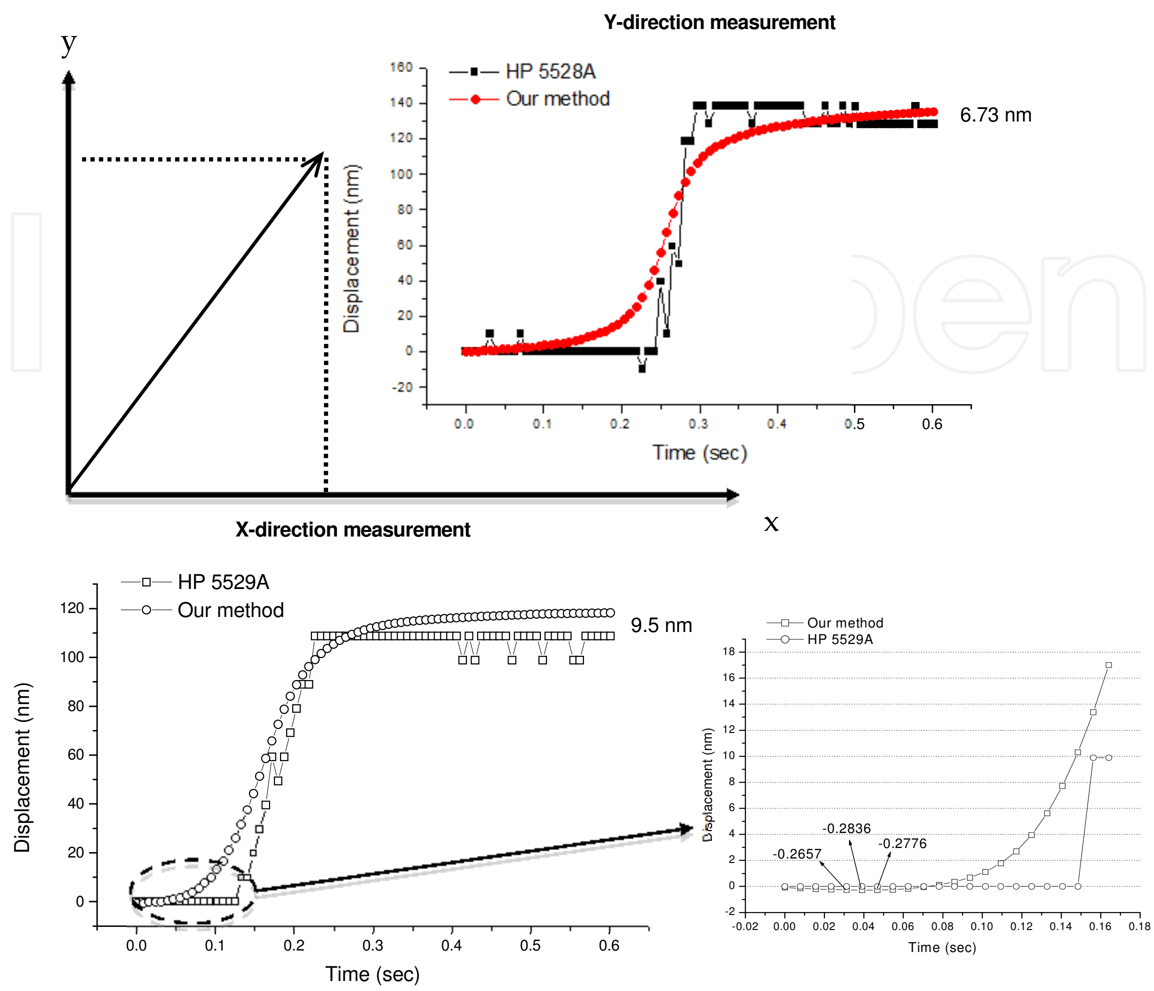

Fig. 11. Displacement measurement of 2-D movement of motorized stage with GHI and HP 5529A.

overlapping area O_1 to O_4; when the grating moves along the y direction, the interference phase changes can be observed from the overlapping area O_5 to O_8. One can use an iris before the focus lens to control the overlapping area. The overlapping areas (O_1 and O_5) are chosen to pass through two polarizers P_1 and P_2 with transmittance axes at 0°. The interference of the light is detected using two detectors D_1 and D_2. The interference signal I_1 and I_2 measured by the detectors D_1 and D_2 can be written as

$$I_1 = 1 + \cos(\omega t - \phi_{x1}), \tag{21a}$$

$$I_2 = 1 + \cos(\omega t - \phi_{y1}). \tag{21b}$$

A polarizer P_3 for which the transmittance axis is at 45° and a detector D_3 are used to measure the intensity of the non-overlapping areas which can be a reference signal I_3 (measured by D_3) and written as

$$I_3 = 1 + \cos(\omega t), \tag{22}$$

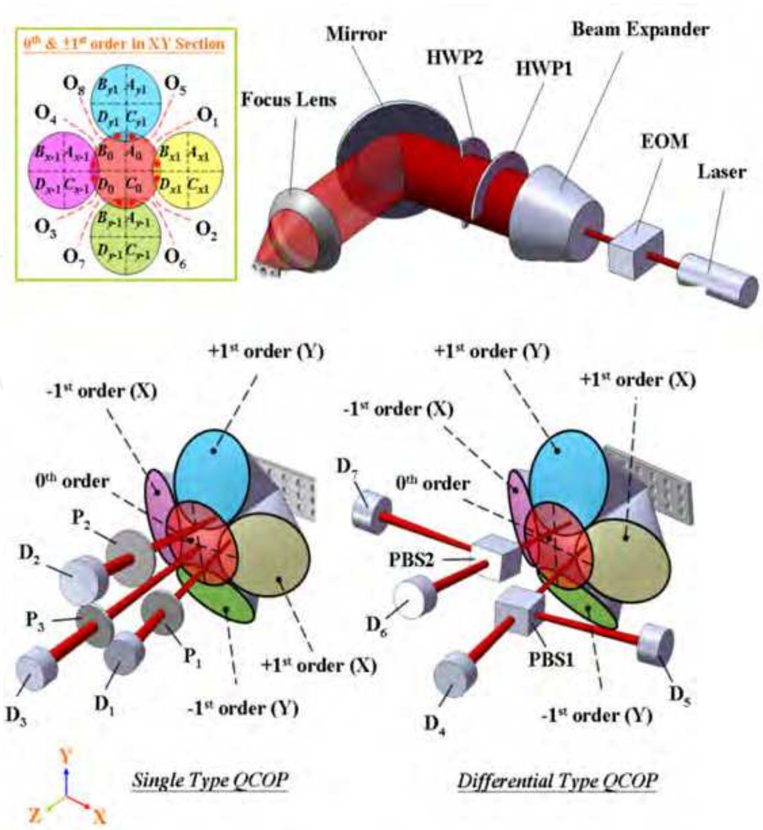

Fig. 12. The schematic of the single type and differential type QCOP heterodyne grating interferometer.

These three signals I_1, I_2, and I_3 are sent into the lock-in amplifier and the phase differences $\Phi_x = \phi_{x1}$ (between I_1 and I_3) and $\Phi_y = \phi_{y1}$ (between I_2 and I_3) are given by

$$\phi_i = \frac{2\pi}{g_i} d_i \quad (i = x, y), \tag{23}$$

where d_i is the displacement in x- and y- directions; g_i is the grating pitch of 2-D grating in x- and y- directions. It is obvious that the 2-D displacement can be obtained as the phase difference and grating pitch of the 2-D grating are given. In the differential type QCOP method, two polarization beam splitters (PBSs) are used to separate the two overlapping beams into four parts. Therefore, the interference signals detected by D_4, D_5, D_6, and D_7 can be written as

$$I_4 = 1 + \cos(\omega t - \phi_{x1}) \text{ and } I_5 = 1 + \cos(\omega t + \phi_{x1}); \quad \text{(for x- direction)} \tag{24a}$$

$$I_6 = 1 + \cos(\omega t - \phi_{y1}) \text{ and } I_7 = 1 + \cos(\omega t + \phi_{y1}). \quad \text{(for y- direction)} \tag{24b}$$

These two pairs signal are sent into the multi-channel lock-in amplifier, the phase differences $\Phi_x = \phi_{x1} - (-\phi_{x1})$ (between I_4 and I_5) and $\Phi_y = \phi_{y1} - (-\phi_{y1})$ (between I_6 and I_7) are 4 times of ϕ_i.

Figure 13 shows a top view of the experimental results in the XY section and the XY stepper moves with a displacement of 1 mm. It is clear that the slight difference between the results measured by the laser encoder and QCOP method. The difference is coming from a tiny angle between the moving direction and the grating, which can be alignment by mounting 2D grating on the rotation stage. In their case, the larger difference was about 12 μm in the y-direction and the smallest difference was about 29 nm in the x- direction for a displacement of 1 mm. Based on the error analysis, if the phase resolution (0.001°) of the lock-in amplifier is considered, the corresponding displacement resolutions of the differential and single type interferometers are estimated to be 9 pm and 4.5 pm for a grating pitch of 3.2 μm, respectively. If only high frequency noise is considered, the measurement resolution of the differential and single type QCOP interferometers can be estimated to be 1.41 nm and 2.52 nm.

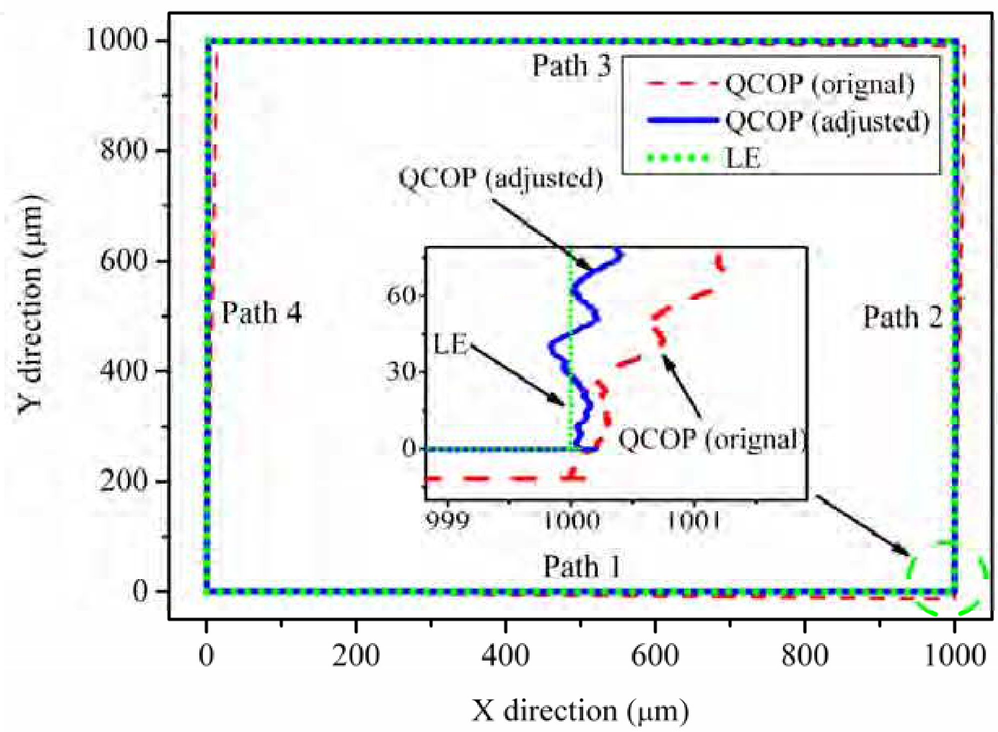

Fig. 13. Displacement measurement of the quadrangular motion with the QCOP method [30].

4. Optical constants measurement with heterodyne interferometer

Optical constants of the materials such as refractive index, birefringence, optical activity, and thickness are significant parameters in material science. There are many methods [9-12, 31-40] can determine those factors, most popular method is ellipsometer [9-12]. Recently, these factors can be obtained by heterodyne interferometer. In this section, we will review some novel methods [31-40] for optical constants measurement with heterodyne interferometer.

C. C. Hsu [32] proposed a novel method for determine the refractive index of the bulk materials with normal incident circular heterodyne interferometer (NICHI) and the schematic diagram is shown in figure 14. The circular heterodyne light source was incident into the modified Twyman-Green interferometer, in which the testing signal reflected from the sample can be interfered and carried by the circular heterodyne light beams. Based on Jones calculation, the interference signal measured by D can be written as

$$I_t = |E_1 + E_2|^2 = I_0[1 + \gamma \cos(\omega t + \phi)], \tag{25}$$

where E_1 and E_2 are the E-field coming from the optical path 1 and path 2 respectively. I_0, γ, and ϕ are the mean intensity, the visibility and the phase of the interference signal, respectively. In additions, they can derive from the Jones calculation and written as

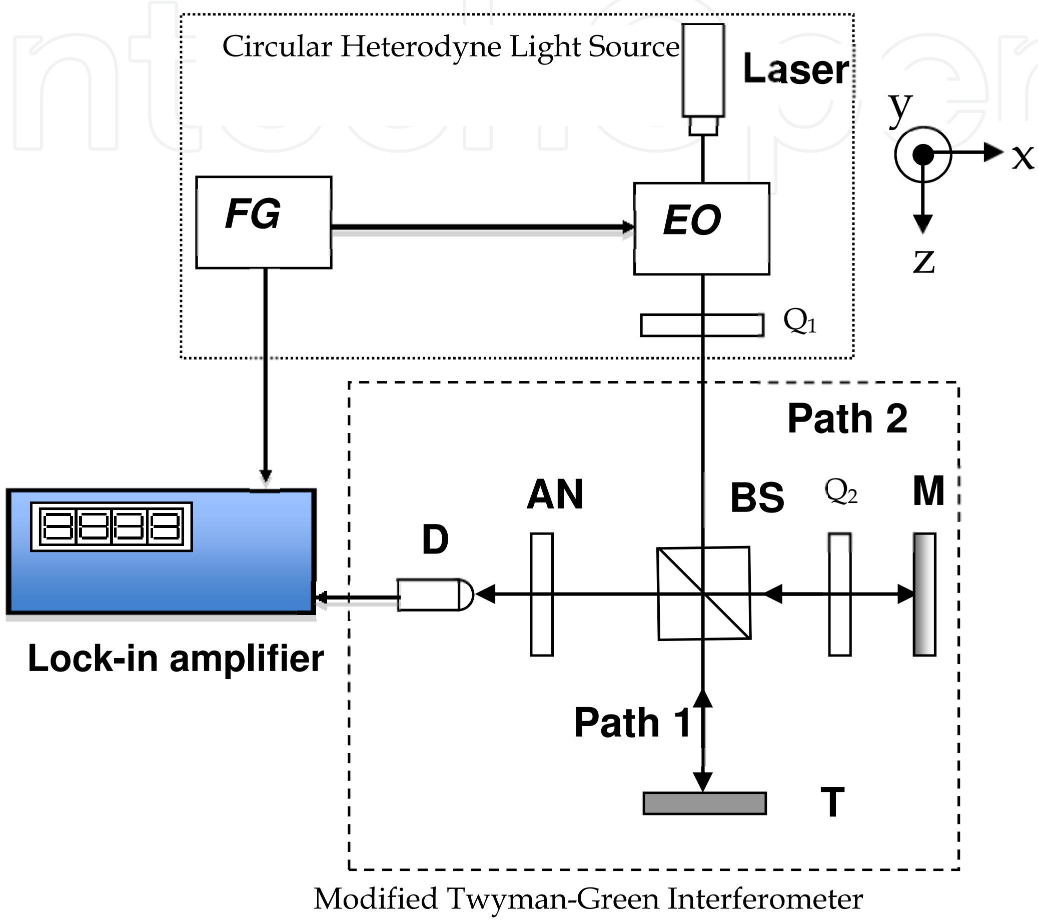

Fig. 14. The optical configuration of normal incident circular heterodyne interferometer [32].

$$I_0 = \left[\frac{1}{2}\left(\frac{n-1}{n+1}\right)^2 + 2{r_m}^2 + 2\left(\frac{n-1}{n+1}\right) r_m \sin 2\alpha \sin(\phi_{d1} - \phi_{d2})\right], \tag{26a}$$

$$\gamma = \frac{\sqrt{A^2+B^2}}{\left[\frac{1}{2}\left(\frac{n-1}{n+1}\right)^2 + 2{r_m}^2 + 2\left(\frac{n-1}{n+1}\right) r_m \sin 2\alpha \sin(\phi_{d1} - \phi_{d2})\right]}, \tag{26b}$$

$$\phi = \tan^{-1}\left(\frac{B}{A}\right), \tag{26c}$$

where the symbols A and B can be written as

$$\mathrm{A} = \frac{1}{2}\left[\left(\frac{n-1}{n+1}\right)^2 - 4{r_m}^2\right] \cdot (\cos^2\alpha - \sin^2\alpha), \tag{27a}$$

$$\mathrm{B} = \frac{1}{2}\left[\left(\frac{n-1}{n+1}\right)^2 - 4{r_m}^2\right] \cdot \sin 2\alpha - 2\frac{n-1}{n+1} r_m, \tag{27b}$$

where r_m is the normal reflection coefficients of the test medium. If the phase can be measured and the reflectivity of mirror is given, the refractive index of the testing sample will be obtained. Furthermore, it is clear that the resolution of refractive index is strongly related to the azimuth angle of analyzer and the reflectivity of the mirror. To derive equation (26) to n, the resolution of refractive index can be written as

$$\Delta n = \frac{1}{\frac{d\phi}{dn}}|\Delta\phi| = [\frac{ac-b}{cd}]|\Delta\phi|, \quad (28)$$

where a, b, c, and d are

$$a = \frac{2[-\frac{4r_m}{(1+n)^2}+\frac{2(n-1)}{(1+n)^3}\sin 2\alpha]}{[\left(\frac{n-1}{1+n}\right)^2-4{r_m}^2][\cos^2\alpha-\sin^2\alpha]}, \quad (29a)$$

$$b = 2\frac{4(n-1)}{(1+n)^3}\left\{\frac{-2(n-1)r_m}{1+n}+\frac{1}{2}[\left(\frac{n-1}{n+1}\right)^2-4{r_m}^2]\cdot\sin 2\alpha\right\}, \quad (29b)$$

$$c = [\left(\frac{n-1}{n+1}\right)^2-4{r_m}^2]^2(\cos^2\alpha-\sin^2\alpha), \quad (29c)$$

$$d = 1+\frac{4\left\{\frac{-2(n-1)r_m}{n+1}+\frac{1}{2}[\left(\frac{n-1}{n+1}\right)^2-4{r_m}^2]\sin 2\alpha\right\}^2}{[\left(\frac{n-1}{n+1}\right)^2-4{r_m}^2]^2[\cos^2\alpha-\sin^2\alpha]^2}. \quad (29d)$$

The simulation results were shown in figure 15 and resolution of the refractive index can be reached 10^{-5} as the suitable experimental conditions were chosen.

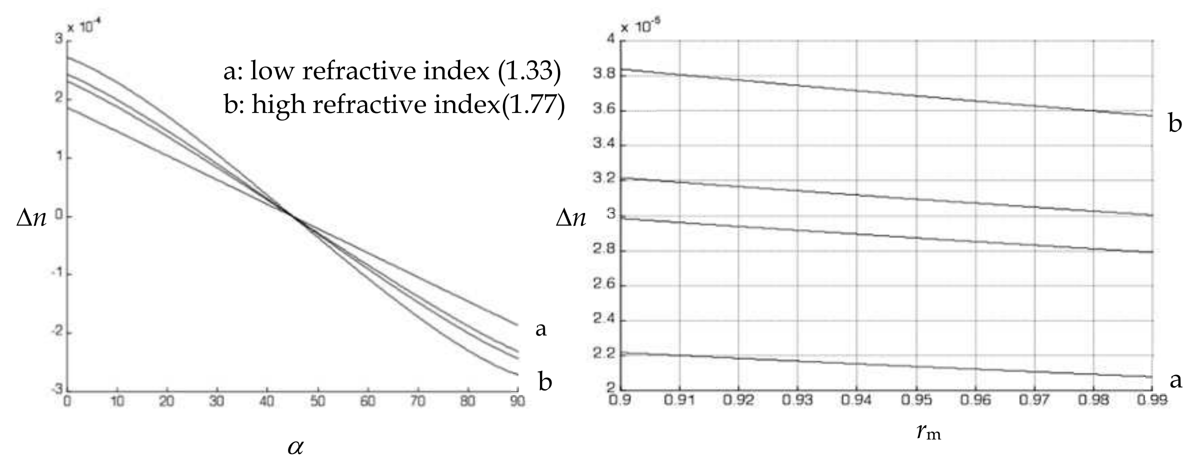

Fig. 15. The relationship between the azimuth angle, reflectivity of the mirror, and resolution of the refractive index [32].

In 2010, Y. L. Chen and D. C. Su [38] developed a full-field refractive index measurement of gradient-index lens with normal incident circular heterodyne interferometer (NICHI). They used high speed CMOS camera to record 2D interference signal and the optical configuration was shown in figure 16.

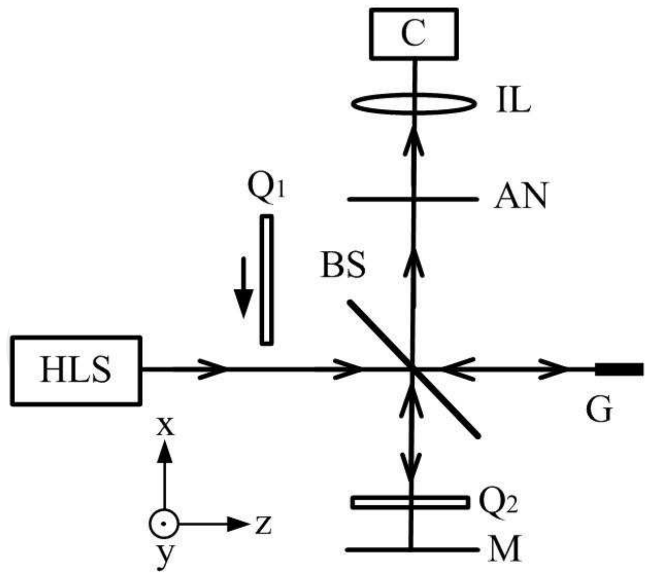

Fig. 16. Optical configuration of full-field normal incident circular heterodyne interferometer [38].

In this interferometer, one is for reference beam (BS→Q_2→M→Q_2→BS→AN→IL→C) and one is for testing beam ((BS→G→BS→AN→IL→C). Here, G means GRIN lens. They were interfere with each other after passing through AN. Before insert the Q_1, the interference signal can be written as

$$I_1 = I_0 + \gamma_1 \cos(2\pi f t + \phi_1)$$

$$= \frac{1}{2}\left\{r^2 + {r_m}^2 - 2 r r_m \cos\left[2\pi f t + \frac{\pi}{2} - (\phi_{d1} - \phi_{d2} + \phi_r)\right]\right\} \tag{30}$$

where I_0 , γ_1 , and ϕ_1 are the mean intensity, visibility, and phase of the interference signal, respectively. Then insert the Q_1, the interference signal can be written as

$$I_2 = [r r_m \sin(\phi_{d1} - \phi_{d2} + \phi_r)] \cos(2\pi f t) + \left|\frac{1}{2}({r_m}^2 - r^2)\right| \cos(2\pi f t) + C, \tag{31a}$$

and

$$\phi_2 = \cot^{-1}\left[\frac{2 r r_m \sin(\phi_{d1} - \phi_{d2} + \phi_r)}{({r_m}^2 - r^2)}\right]. \tag{31b}$$

It is obvious that the refractive index of the GRIN lens G can be the function of ϕ_1 and ϕ_2 which expressed as

$$n = \frac{\cot\phi_2 - r_m \cos\phi_1 + r_m\sqrt{\cos^2\phi_1 + \cot^2\phi_2}}{\cot\phi_2 + r_m \cos\phi_1 - r_m\sqrt{\cos^2\phi_1 + \cot^2\phi_2}}. \tag{32}$$

Therefore, for a specified r_m, ϕ_1 and ϕ_2 are given by the measurement, the refractive index of GRIN lens can be obtained.

For full-filed heterodyne phase detection can be realized with three-parameter sine wave fitting method that proposed by IEEE standards 1241-2000. The fitting equation has the form of

$$I(t) = \sqrt{{A_0}^2 + {B_0}^2}\cos(2\pi f t + \varphi) + C_0, \tag{33a}$$

and

$$\varphi = \tan^{-1}\left(\frac{-B_0}{A_0}\right). \tag{33b}$$

where A_0 , B_0 , and C_0 are real numbers and they can be derived with the least-square method. And finally the phase of the all pixels on the CCD camera can be obtained. Based on their method, they demonstrated the two dimensional refractive index distribution of the GRIN lens and showed in figure 17.

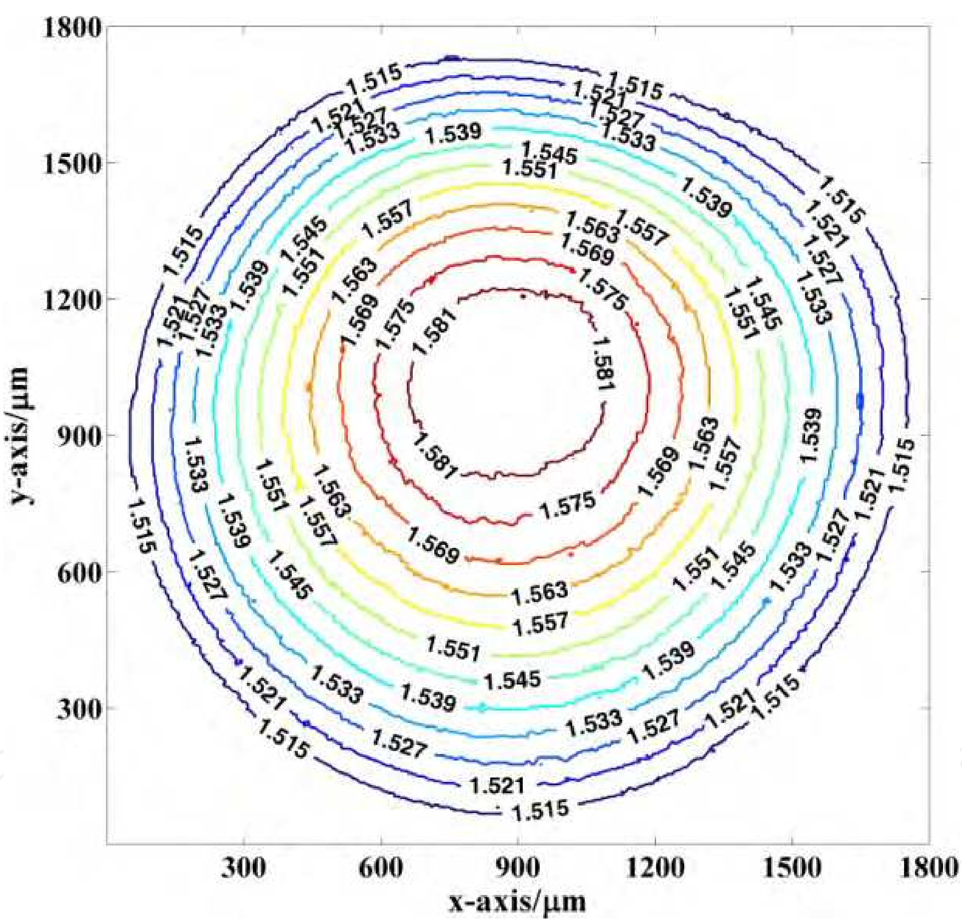

Fig. 17. The refractive index contour of GRIN lens measured by full-field NICHI [38].

For the measurement of the optical constants of the thin film, K. H. Chen and C. C. Hsu [33] proposed a circular heterodyne refractometer. The optical configuration was shown in figure 18. The circular heterodyne light source was incident onto the sample at θ_0 and the light will be partially transmitted and reflected at the interface between the thin film and substrate. If the transmission axis of AN is located at α with respect to the x-axis, then the E-field of the light arriving at D is given

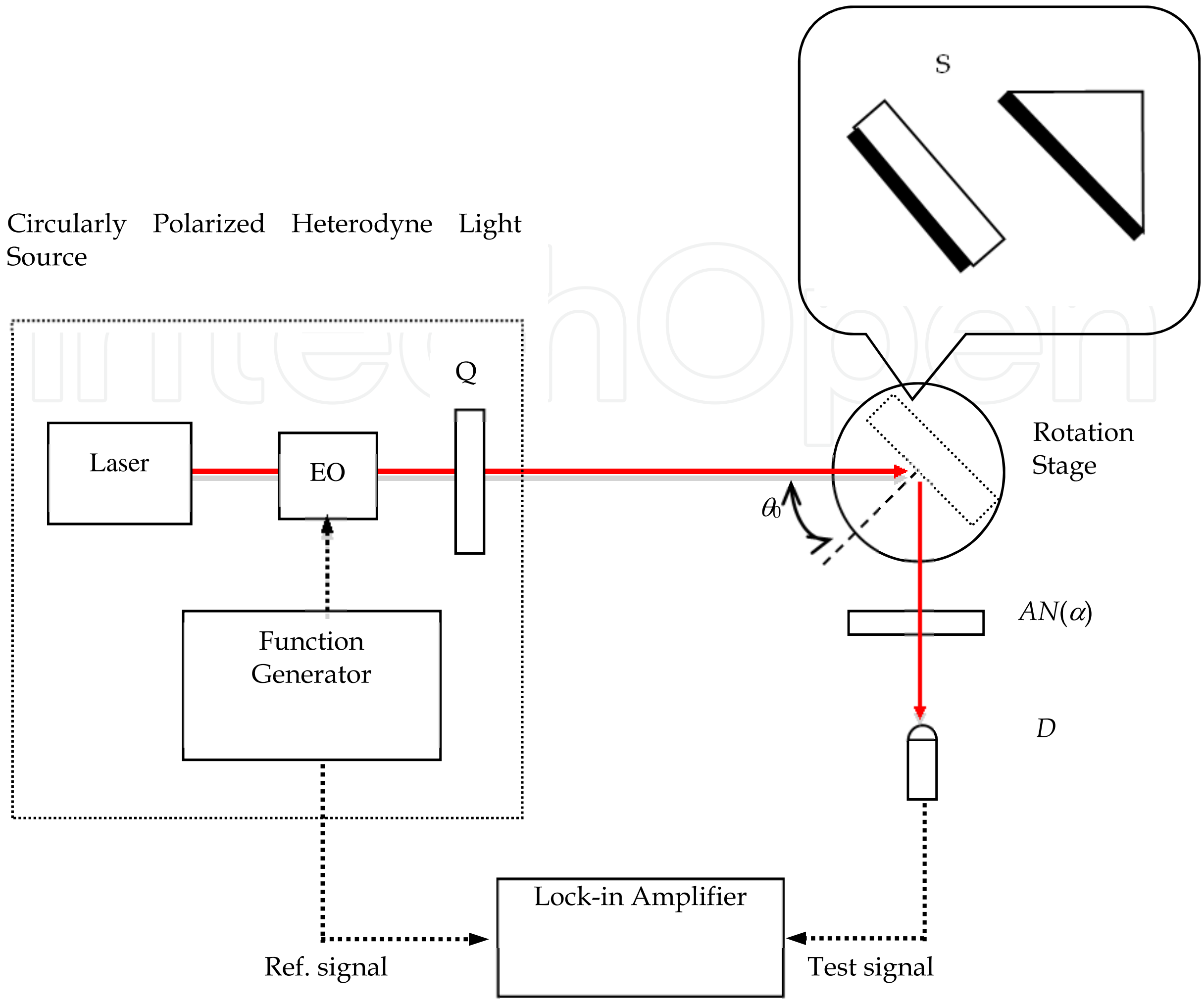

Fig. 18. The circular heterodyne refractor.

$$E_t = \begin{pmatrix} \cos^2 \alpha & \sin\alpha\cos\alpha \\ \sin\alpha\cos\alpha & \sin^2\alpha \end{pmatrix} \begin{pmatrix} r_p & 0 \\ 0 & r_s \end{pmatrix} \begin{pmatrix} \cos\frac{\omega t}{2} \\ -\sin\frac{\omega t}{2} \end{pmatrix} = \begin{pmatrix} r_p \cos^2\alpha \cos\frac{\omega t}{2} - r_s \sin\alpha\cos\alpha \sin\frac{\omega t}{2} \\ r_p \sin\alpha\cos\alpha\cos\frac{\omega t}{2} - r_s \sin^2\alpha \sin\frac{\omega t}{2} \end{pmatrix}. \quad (34)$$

Therefore, the testing signal detected by the detector D can be written as

$$I_t = |E_t|^2 = I_0[1 + \frac{\sqrt{A^2+B^2}}{I_0}\cos(\omega t + \phi)], \quad (35)$$

where I_0 and γ are the bias intensity and the visibility of the signal, and ϕ is the phase difference between the p- and s- polarizations coming from the reflection of the sample. They can be expressed as

$$I_0 = \frac{1}{2}(|r_p|^2 \cos^2\alpha + |r_s|^2 \sin^2\alpha), \quad (36a)$$

$$A = \frac{1}{2}(|r_p|^2 \cos^2\alpha - |r_s|^2 \sin^2\alpha), \quad (36b)$$

$$B = \frac{1}{2}(r_p r_s^* + r_s r_p^*) \sin\alpha\cos\alpha, \quad (36c)$$

and

$$\phi = \tan^{-1}(\frac{B}{A}) = \tan^{-1}[\frac{(r_p r_s^* + r_s r_p^*) \sin\alpha \cos\alpha}{(|r_p|^2 \cos^2\alpha - |r_s|^2 \sin^2\alpha)}]. \tag{36d}$$

The symbols r_p and r_s are the Fresnel equation (as equation 13); r_p^* and r_s^* are the conjugates of r_p and r_s, respectively. It is obvious that the phase difference coming from the samples are function of the incident angle and the transmission axis of the analyzer *AN*. In practice, one can adjust three transmission axis of the analyzer at fixed incident angle or change three different incident angles with fixed transmission axis of the analyzer to get the corresponding phase difference ϕ. Therefore, substitute the phase difference into equation (36d) the optical constants of the sample can be obtained. According to Chen's results, they can successfully measure the thin metal film deposited on the glass substrate with lower measurement errors, which are 10^{-3} for the complex refractive index and 10^{-1} nm for the thickness.

Birefrigent crystals (BC) have been used to fabricate polarization optical components for a long time. To enhance their qualities and performances, it is necessary to determine the optical axis (OA) and measure the extraordinary index n_e and the ordinary index n_o accurately. There are many methods proposed to measure these parameters of the birefrigent crystal. Huang *et al.* [39] measured (n_e, n_o) of the wedge-shaped birefrigent crystal with transmission-type method. Therefore, the accuracy of thickness, flatness and parallelism of the two opposite sides of the birefrigent crystals are strongly required. D. C. Su and C. C. Hsu [37] proposed a novel method for measuring the extraordinary index n_e, the ordinary index n_o, and the azimuth angle of the birefrigent crystal with single apparatus which described in figure 19. Based on the circular heterodyne interferometer (CHI) and replaced the sample by the birefrigent crystal, the Jones vector of the E-field detected by *D* can be written as

$$E_t = AN(\beta) \cdot \begin{bmatrix} r_{pp} & r_{ps} \\ r_{sp} & r_{ss} \end{bmatrix} \cdot E_i$$

$$= \left(\left(r_{pp} \cos\beta + r_{sp} \sin\beta \right) \cos\frac{\omega t}{2} - \left(r_{ps} \cos\beta + r_{ss} \sin\beta \right) \sin\frac{\omega t}{2} \right) \begin{pmatrix} \cos\beta \\ \sin\beta \end{pmatrix} \tag{37}$$

where S is the Jones matrix for BC, r_{pp} and r_{ss} are the direct-reflection coefficients, and r_{ps} and r_{sp} are the cross-reflection coefficients [14], respectively. Based on Fresnel equations, r_{pp}, r_{ss}, r_{ps} and r_{sp} are the function of the n_e, n_o, and azimuth angle α of the birefrigent crystal. Therefore, the intensity of the testing signal can be expressed

$$I_t = |E_t|^2 = \frac{\left(r_{pp} \cos\beta + r_{sp} \sin\beta\right)^2 + \left(r_{ps} \cos\beta + r_{ss} \sin\beta\right)^2}{2} [1 + \cos(\omega t + \phi)], \tag{38a}$$

and

$$\phi = \tan^{-1} \left(\frac{2\left(r_{pp} \cos\beta + r_{sp} \sin\beta\right)\left(r_{ps} \cos\beta + r_{ss} \sin\beta\right)}{\left(r_{pp} \cos\beta + r_{sp} \sin\beta\right)^2 + \left(r_{ps} \cos\beta + r_{ss} \sin\beta\right)^2} \right). \tag{38b}$$

Theoretically, it is difficult to obtain the n_e, n_o, and azimuth angle α of the birefrigent crystal by substituting the phase difference, which is arbitrary choose the measurement conditions

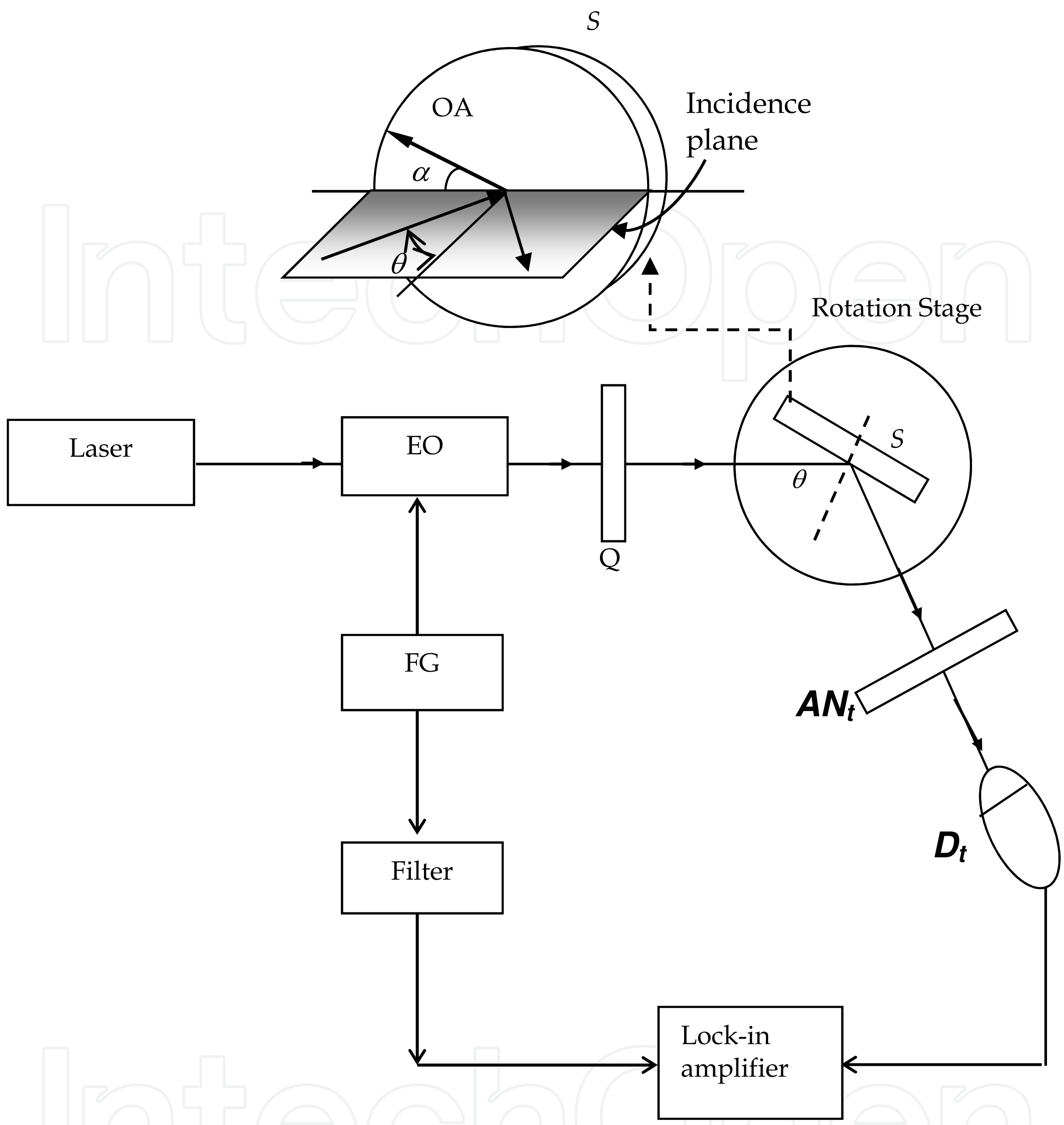

Fig. 19. Optical configuration of the determination of the optical properties of birefrigent crystal with CHI.

of the incident angle and azimuth angle of the analyzer, into equation (38b). Therefore, Su developed a sequence for determining these parameters. First, let azimuth angle β of analyzer equal to 0° and phase difference can be written as

$$\phi = \tan^{-1}\left(\frac{2r_{pp}r_{ps}}{{r_{pp}}^2 - {r_{ps}}^2}\right). \tag{39}$$

As azimuth angle α of the birefrigent crystal at 0° or 90°, r_{ps} and r_{sp} will be equal to 0, and phase difference ϕ is equal to 0. But in this period, one cannot determine the azimuth angle α of brifrigent crystal exactly at 0° or 90°.

Second, fixed the azimuth angle of the birefrigent crystal and rotated azimuth angle β of analyzer to nonzero position. The phase difference ϕ can be expressed as

$$\phi = \tan^{-1}\left(\frac{\sin 2\beta \cdot r_{pp} r_{ps}}{r_{pp}{}^2 \cos^2\beta - r_{ss}{}^2 \sin^2\beta}\right). \tag{40}$$

At this period, the r_{pp} and r_{ss} will be under one of the conditions (i) α=90°or (ii) α=0°. Hence, we solved the n_e and n_o under conditions (i) and (ii) with two different incident angles.

Third, determine the correct solution with two justifications. (1) Rationality of the solution: In general, both n_e and n_o are within the range 1 and 5. If any estimated data of n_e and n_o is not within this range, it is obvious that the estimated data may be incorrect. (2) Comparison between n_e and n_o: Either a positive or negative crystal is tested, all two pairs of solutions of either group should meet with only either $n_e > n_o$ or $n_e < n_o$. If not, then that group is incorrect.

Based on Su's procedure, they have successfully determined the n_e, n_o, and azimuth angle α of the birefrigent crystal, which were positive crystal (quartz) and negative crystal (calcite), with lower error of the refractive index (~ 10^{-3}) and azimuth angle (~0.1°) of BC.

J. F. Lin *et al* [40] proposed a transmission type circular heterodyne interferometer to determine the rotation angle of chiral medium (glucose solution). The optical setup was shown in figure 20 and the E-field of the testing signal derived from Jones calculation is given

$$\mathrm{E} = \mathrm{A}(0)\cdot \mathrm{S}(\theta)\cdot Q_1(45)\cdot EO(90)\cdot P(45)\cdot E_{in}$$

$$= \begin{bmatrix}1 & 0\\ 0 & 0\end{bmatrix}\begin{bmatrix}\cos\theta & \sin\theta\\ -\sin\theta & \cos\theta\end{bmatrix}\begin{pmatrix}\frac{1-i}{2} & \frac{1+i}{2}\\ \frac{1+i}{2} & \frac{1-i}{2}\end{pmatrix}\begin{bmatrix}e^{-i\omega t/2} & 0\\ 0 & e^{-\omega t/2}\end{bmatrix}\begin{bmatrix}\frac{1}{2} & \frac{1}{2}\\ \frac{1}{2} & \frac{1}{2}\end{bmatrix}\begin{bmatrix}0\\ E_0 e^{iw_0 t}\end{bmatrix}, \tag{41}$$

where θ is the optical rotation angle of the chiral medium. And the intensity of the testing signal detected by the photodetector can be derived and written as

$$I_t = I_{dc}[1-\sin(\omega t - 2\theta)], \tag{42}$$

Compare with the reference signal by lock-in amplifier, the phase difference between the reference and testing signals can be obtained. Theoretically, the optical rotation angle is strongly related to the concentration, temperature, and propagation length of the chiral medium (glucose solution). And that can be expressed as

$$C = \frac{100\theta}{L[\theta]}, \tag{43}$$

where the glucose concentration C (g/dl) in a liquid solution, θ (degree) is optical rotation angle, L (decimeter) is the propagation length in chiral medium.

Figure 21 showed that the optical rotation angle of the glucose solution which the concentration was varied from 0 to 1.2 g/dl. Their results showed the good linearity and high sensitivity which can achieve 0.273° /g/dl.

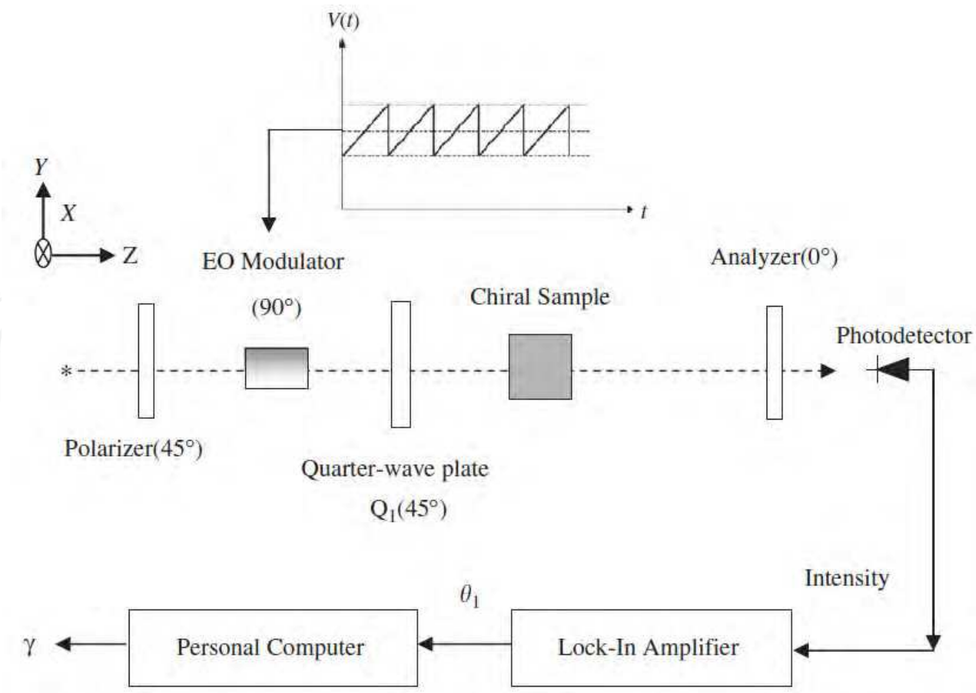

Fig. 20. Schematic diagram of circular heterodyne interferometer for measuring the optical rotation angle in a chiral medium [40].

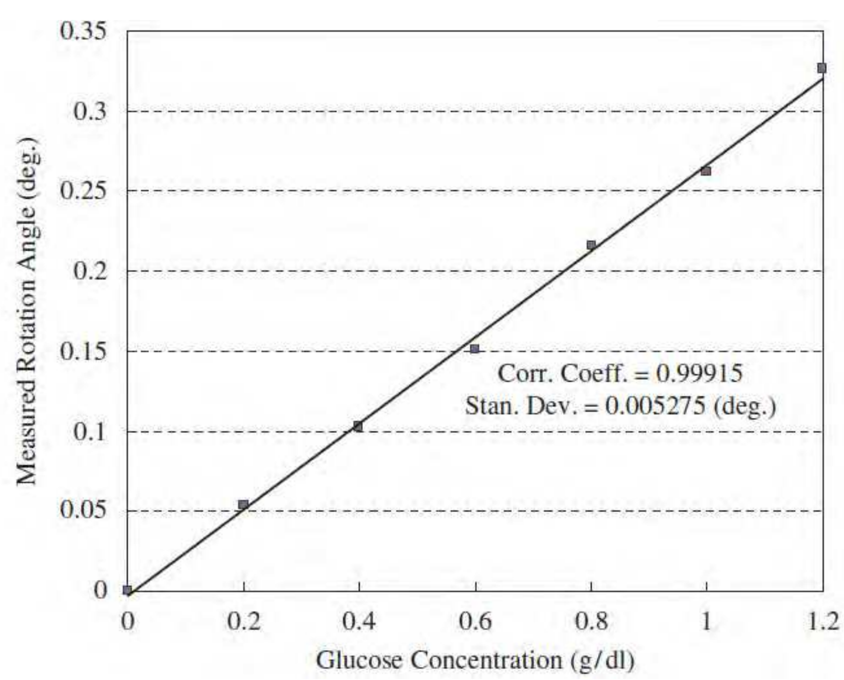

Fig. 21. Optical rotation angle of glucose solution with concentration variation [40].

5. Concentration measurement with heterodyne interferometer

The concentration of solution is an important factor in food, chemical and biochemical industrial, especially in health care and disease prevention. For example, the blood glucose concentration is related to the diabetes. To control the blood glucose concentration within the normal level is critical issue to the diabetic daily care. Therefore, many researchers developed novel methods for measuring the solution concentration. Because of the advantages of the optical method such as high sensitivity, high resolution, non-contact, and quick response, optical measurement method become more popular in past few decades. And these methods can roughly divide into fiber type sensor [41, 44-45, 49] and non-fiber type sensor [42-43, 46-48, 50]. In this section, we will review some recent development in both type sensors for measuring concentration of the specific chemical compound [41-50].

M. H. Chiu [41] developed a D-shape fiber sensor with SPR property and integrated with heterodyne interferometer which could detect variation in the alcohol concentration of 2%. The optical setup was shown in figure 22. The heterodyne light source was guided into the sensor and suffered the attenuate total reflection (ATR) at the sensing region. Because of the refractive index of the sample will be varied as the concentration changed. And induce the phase difference between the p- and s- polarizations. To measure the phase difference can be obtained the concentration variation of the sample.

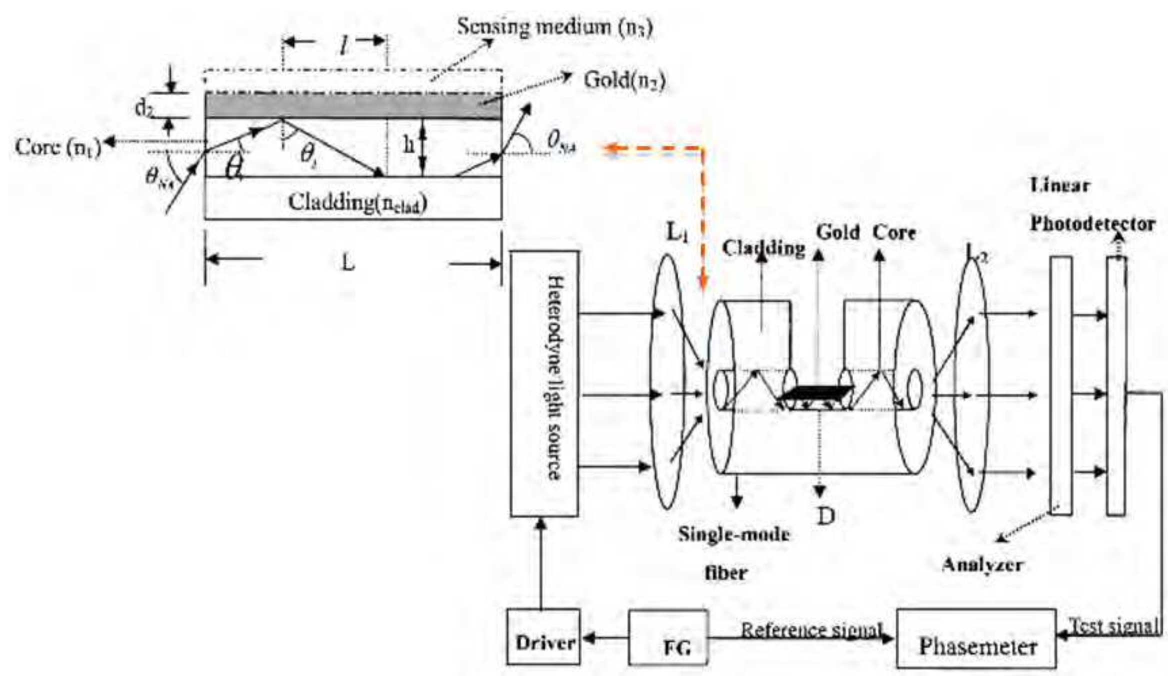

Fig. 22. The scheme of the D-shape fiber sensor [41].

Figure 22 shows that the testing signal detected by photodetector and sent into the phasemeter. Therefore, the interference signal can be written as

$$I(t) = I_0\left\{1 + V\cos\left[\omega t + \left(\frac{L(\phi_p-\phi_s)}{2h\tan\theta_i}\right)\right]\right\}, \tag{44}$$

where I_0 and V are the average intensity and visibility; L and h are the sensing length and core diameter; $(\phi_p\text{-}\phi_s)$ is the phase difference between p- and s- polarizations; θ_i is the incident angle at the interface between fiber core and metal film. Based on the Fresnel equation, one can derive the $(\phi_p\text{-}\phi_s)$ from the amplitude reflection coefficient under ATR condition and it is obvious that $(\phi_p\text{-}\phi_s)$ is the function of the refractive index of the sensing medium. Figure 23 shows that the results measured by the D-shape fiber sensor for different concentration of the alcohol.

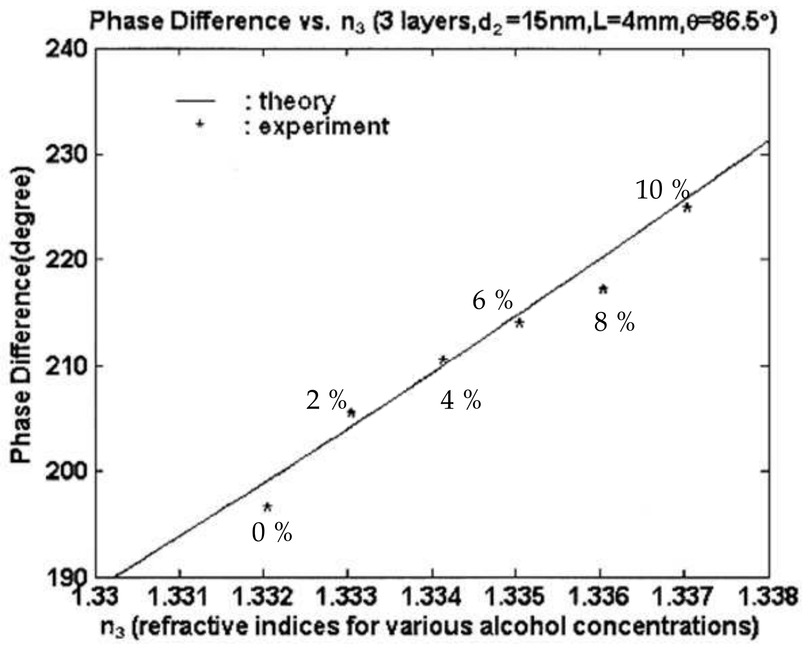

Fig. 23. The experiment result of different concentration of alcohol measured by D-shape fiber sensor [41].

In Chiu's results, they can observe the concentration variation 2 %, in which the corresponding refractive index variation is about 0.0009. Based on error analysis, their method can be reached 2×10^{-6} refractive index unit.

Recently, T. Q. Lin [44] and C. C. Hsu [45] developed a fiber sensor which immobilized glucose oxidase (GOx) on the fiber core for measuring the glucose concentration in serum and phosphate buffer solution (PBS). Their measurement method integrated the fiber sensor and heterodyne interferometer which showed in figure 24.

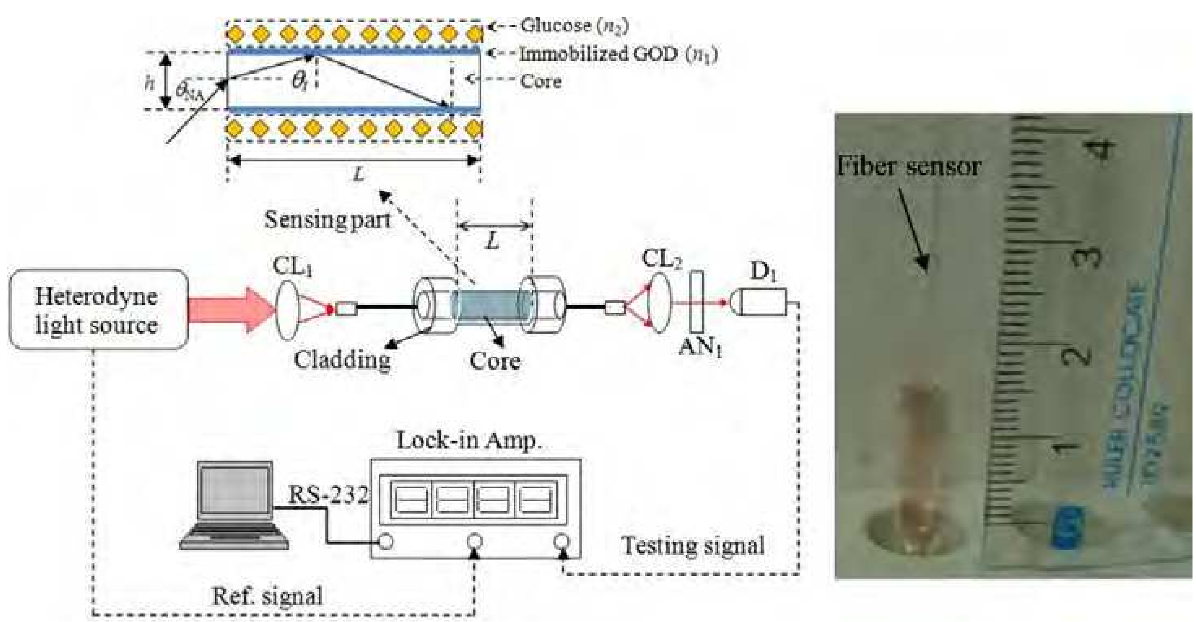

Fig. 24. Schematic diagram of the measurement system and preliminary test of the glucose fiber sensor [44].

As the heterodyne light source enters the sensing part, the light beam undergoes total internal reflection (TIR) and the phase difference between the p- and s- polarization states can be written as

$$\phi_t = m\phi_{TIR} = \frac{L}{h\tan\theta_t}\cdot\tan^{-1}\left(\frac{\sqrt{\sin^2\theta_t-(\frac{n_2}{n_1})^2}}{\tan\theta_t\cdot\sin\theta_t}\right), \tag{45}$$

where n_1 and n_2 are the refractive indices of the immobilized GOx and the testing solution. θ_t and m are the incident angle and the number of TIRs that occur at the interface between the GOx and the testing solution. After dripping the testing sample onto the sensor, the phase will vary as the glucose reacts with the GOx to be converted into gluconic acid and hydrogen peroxide. The chemical reaction can be formulated as follows:

$$\text{Glucose} + O_2 \xrightarrow{\text{GOx}} \text{gluconic acid} + H_2O_2. \tag{46}$$

It means that the refractive index (n_2) will change and consequently the phase will change. Besides, the refractive index n_2 is a function of the concentration of the testing sample. Different concentration of the solution has different refractive index. Therefore, one can determine the concentration variation by measuring the phase variation. In their methods, the phase difference can be carried in the heterodyne interference signal and written as

$$I_t = I_0[1+\cos(\omega t)+\phi_t].$$

To deserve to be mentioned, they found that the pH property between the testing sample and sensor is critical issue for rapid measurement. Figure 25 shows that the response time and response efficiency of the fiber sensor. It is clear that the response time for measuring glucose solution was shorter than those for serum measurement. And the response efficiency for measuring glucose solution was faster than those for serum measurement at different GOx concentration.

Based on their results, this fiber sensor has good linearity of the calibration curve for glucose solution and serum sample. And they showed the best resolutions were 0.1 and 0.136 mg/dl for glucose solution and serum based sample, respectively.

One of the non-fiber type sensors is SPR (surface Plasmon resonance) sensor which has been applied in field such as pharmaceutical development and life sciences. And SPR provides ultra high sensitivity for detecting tiny refractive index (RI) changes or other quantities which can be converted into an equivalent RI. The heterodyne interferometer detects the SPR phase by using a Zeeman laser or optical modulator, such as an acousto-optic modulator or electro-optic modulator and has been reported in the literature. Heterodyne phase detection techniques offer the high measurement performance high sensitivity and high resolution in real-time. J. Y. Lee [43] proposed wavelength-modulation circular heterodyne interferometer (WMCHI) with SPR sensor for measuring the different concentration of alcohol. The diagram of the WMCHI is shown in figure 26.

The SPR sensor had the Kretschmann configuration consists of a BK7 prism coated with a 50 nm gold film and integrated with micro-fluid channel which used to inject the testing

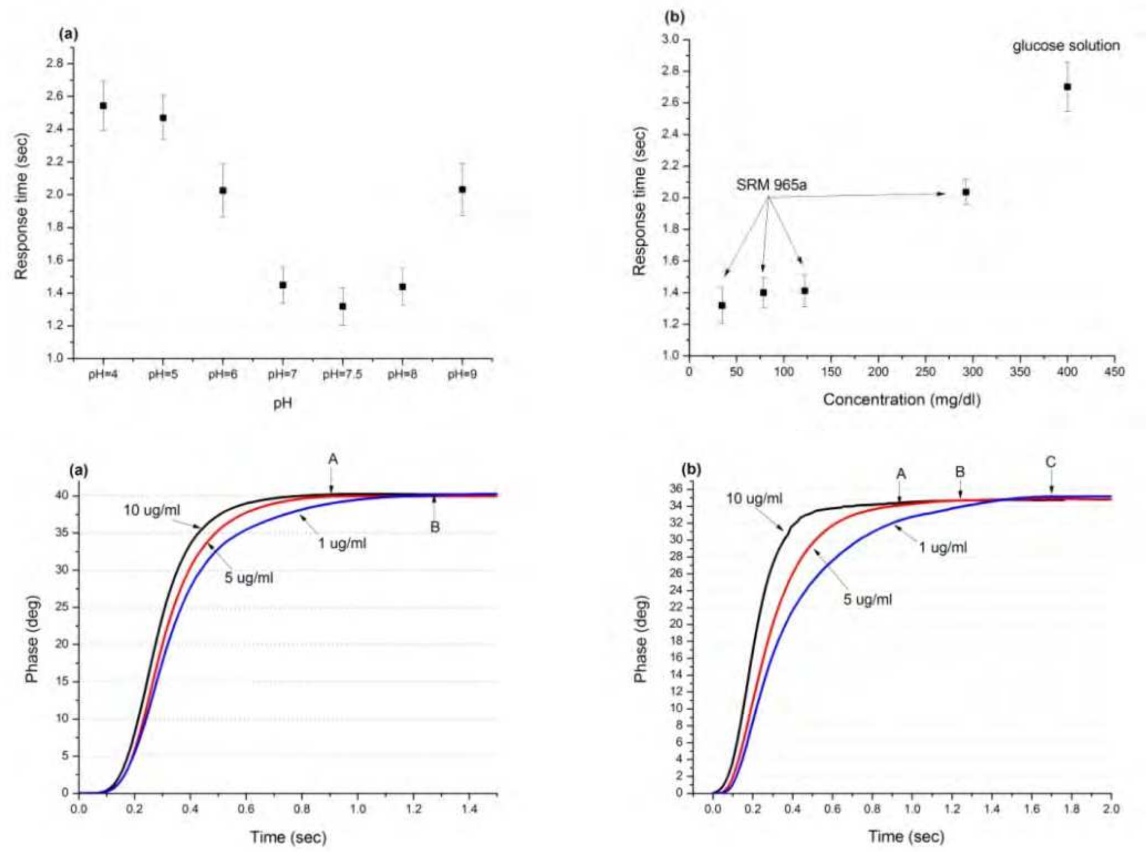

Fig. 25. The response time and response efficiency of the fiber sensor for measuring both glucose solution and human serum [44].

sample. The E-field detected by D_1 and D_2 can be written as

$$E_1 = P(45°) \cdot J_{SPR} \cdot J_Q(45°) \cdot E_h$$

$$= \frac{1}{2}\begin{bmatrix} 1 & 1 \\ 1 & 1 \end{bmatrix} \begin{bmatrix} |r_p|e^{i\phi p} & 0 \\ 0 & |r_s|e^{i\phi s} \end{bmatrix} \frac{1}{\sqrt{2}} \begin{bmatrix} 1 & i \\ i & 1 \end{bmatrix} \begin{bmatrix} e^{i(\phi_0 - \omega t)/2} \\ e^{-i(\phi_0 - \omega t)/2} \end{bmatrix}$$

$$= \frac{1}{2\sqrt{2}} \left[\left(|r_p|e^{i\phi p} + i|r_s|e^{i\phi s} \right) e^{\frac{i(\phi_0 - \omega t)}{2}} + \left(i|r_p|e^{i\phi p} + |r_s|e^{i\phi s} \right) e^{-\frac{i(\phi_0 - \omega t)}{2}} \right] \begin{bmatrix} 1 \\ 1 \end{bmatrix}, \tag{47a}$$

and

$$E_2 = P(-45°) \cdot J_{SPR} \cdot J_Q(45°) \cdot E_h$$

$$= \frac{1}{2\sqrt{2}} \left[\left(|r_p|e^{i\phi p} + i|r_s|e^{i\phi s} \right) e^{\frac{i(\phi_0 - \omega t)}{2}} + \left(i|r_p|e^{i\phi p} + |r_s|e^{i\phi s} \right) e^{-\frac{i(\phi_0 - \omega t)}{2}} \right] \begin{bmatrix} 1 \\ -1 \end{bmatrix}, \tag{47b}$$

where J_{SPR} is the Jones matrix of SPR sensor. They became two testing signals and sent into lock-in amplifier which can obtained the phase difference between them. The phase difference Φ of these two signals is obtained as

$$\Phi = \left(\Phi_0 + \tan^{-1}\frac{B}{A} \right) - \left(\Phi_0 - \tan^{-1}\frac{B}{A} \right) = 2\tan^{-1}\left(\frac{|r_p|^2 - |r_s|^2}{2|r_p||r_s|\cos\phi} \right). \tag{48}$$

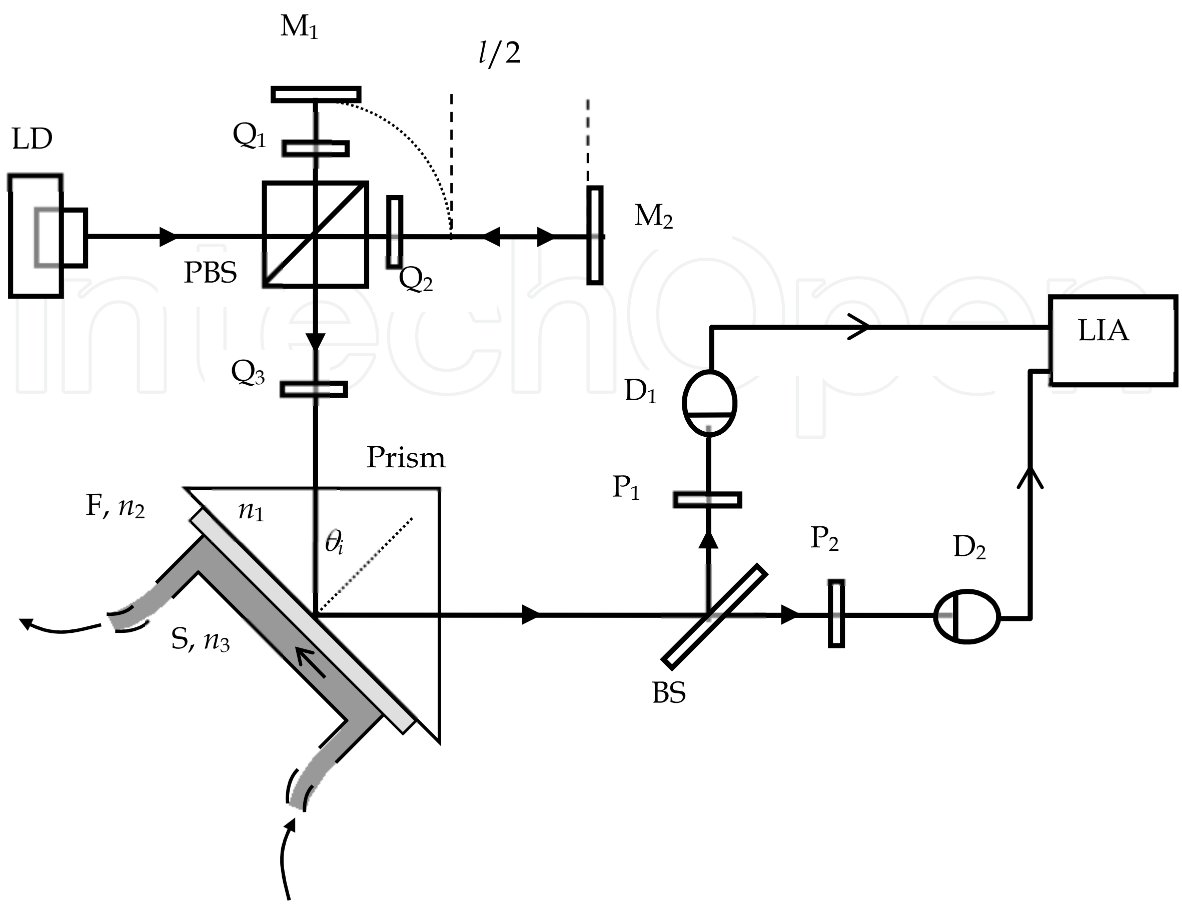

Fig. 26 Schematic diagram of WMCHI for different concentration measurement [43].

Based on equation (44), it is clear that the resonant angles for ϕ and Φ are different. Obviously, Φ is the function of r_p, r_s and ϕ which varies with the refractive index of sample n_3 and the incident angle. The relationship between ϕ and Φ and the incident angle was shown in figure 27 It is obvious that the maximum of Φ is larger than that of ϕ. On the other hand, Φ can be larger than 10,000 in the incident angle interval between 66.25° and 66.75°. This means that Lee's method has a high angle toleration and larger dynamic range.

C. Chou [42] proposed a novel pair surface plasma wave biosensor which provided a larger dynamic measurement range for effective refractive index. In their system, it can avoid excess noise coming from laser intensity fluctuation and environment disturbance. It is important to retain the amplitude stability in this method for high detection sensitivity. Figure 28 showed the amplitude sensitivity PSPR method. In this figure, PBS separated the pair of p-polarization waves and the pair of s-polarization waves, which can be optical heterodyne interference signal at the photodetectors D_p and D_s. Then these two signals can be expressed as

$$I_{p1+p2}(\Delta\omega t) = A_{p1}A_{p2}\cos(\Delta\omega t + \phi_p), \tag{49a}$$

$$I_{s1+s2}(\Delta\omega t) = A_{s1}A_{s2}\cos(\Delta\omega t + \phi_s), \tag{49b}$$

where A_{P1} and A_{P2} are the attenuated amplitudes of the reflected P_1 and P_2 waves respectively; A_{S1} and A_{S2} are the attenuated amplitudes of the reflected S_1 and S_2 waves

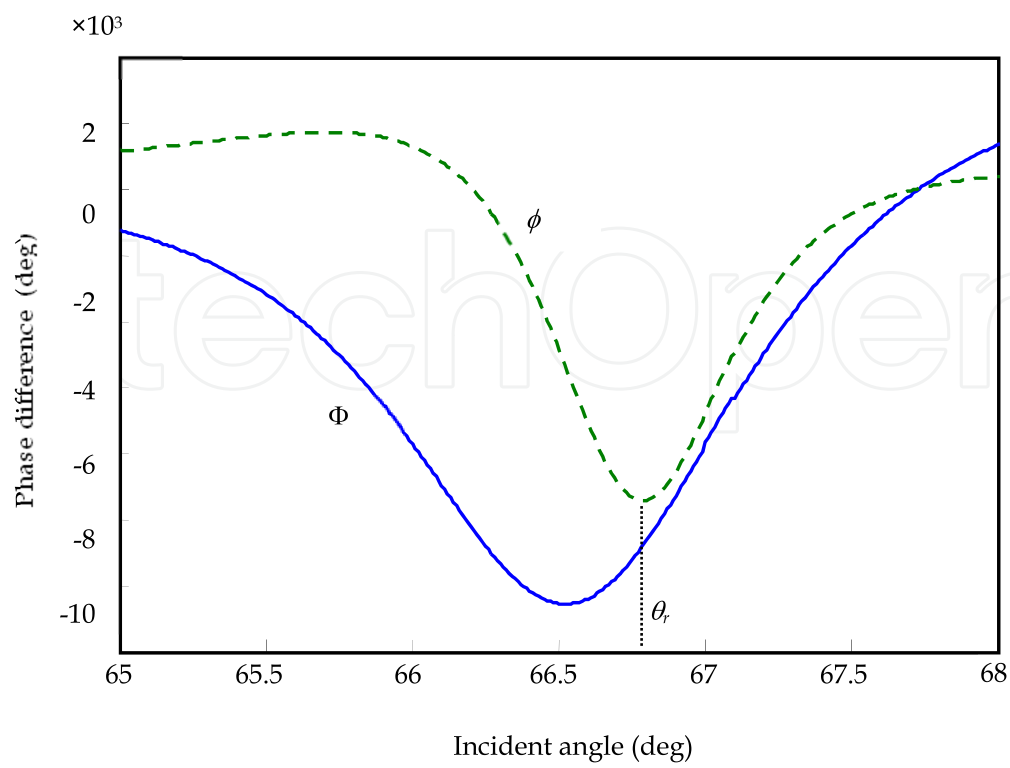

Fig. 27. The relationship between ϕ and Φ and the incident angle [43].

respectively. ϕ_P and ϕ_S are the phase differences of the reflected P and P and the reflected S and S waves respectively. In equation (49), ϕ_P and ϕ_S are equal to 0 and these two interference signals will remain at maximum intensity under the SPR proceeded.

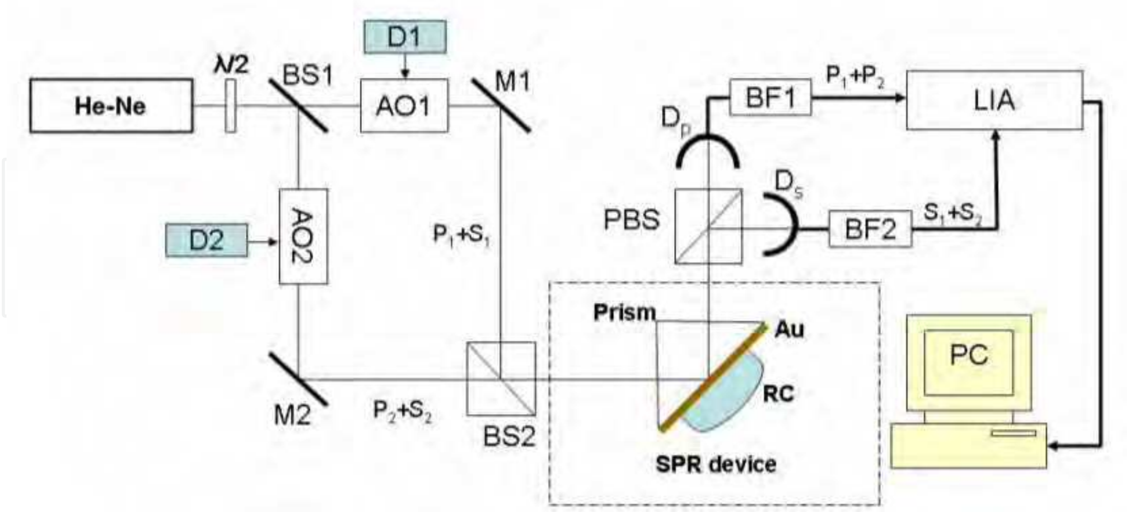

Fig. 28. The schematic of the amplitude sensitivity PSPR [42].

Based on this method, Chou demonstrated three different testing samples with concentration variation which were sucrose, glycerin-water solution, and rabbit anti-mouse IgG. In figure 29, the best of these sample are 8×10^{-8}, 7.6×10^{-7}, and 2×10^{-9}, respectively.

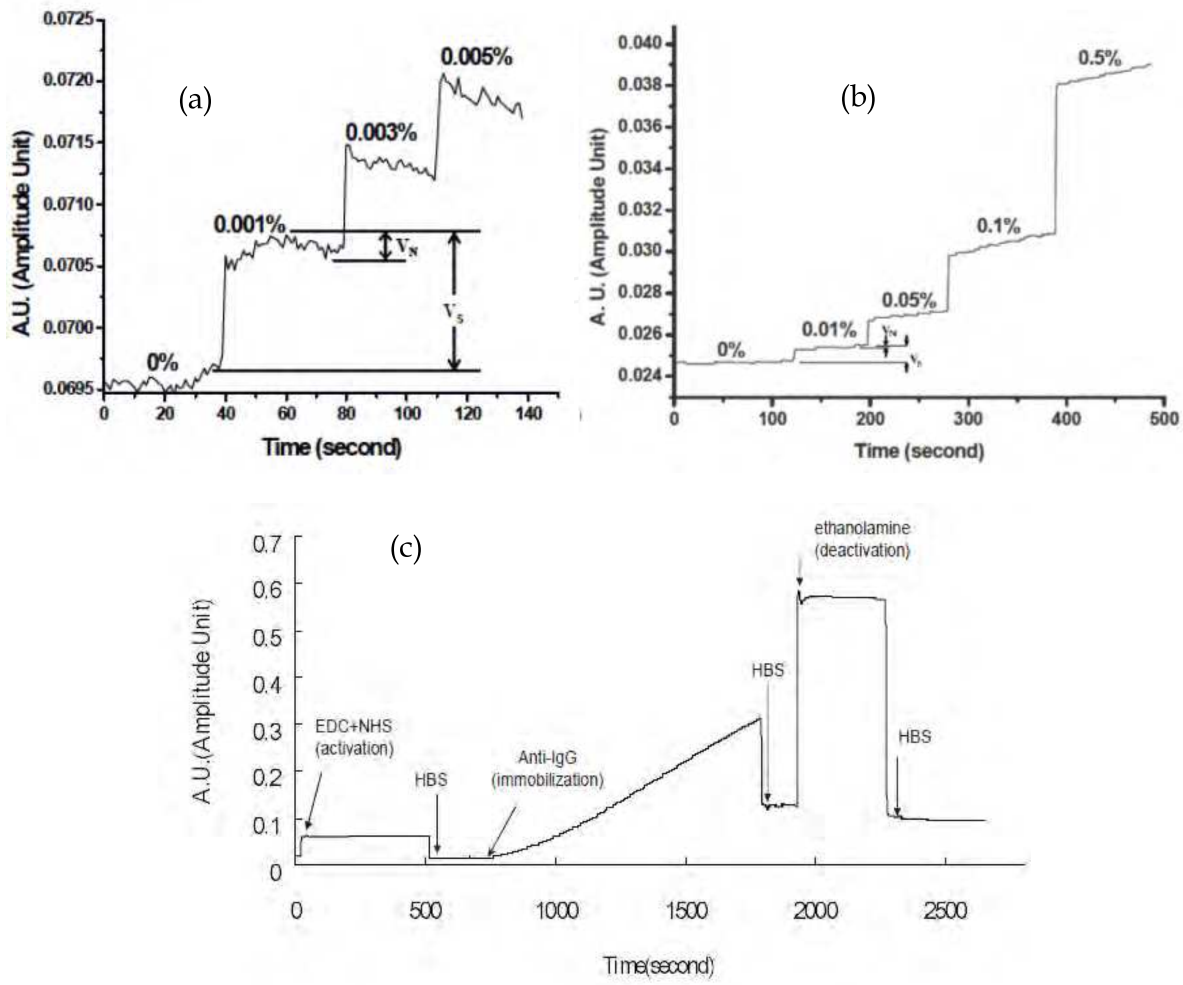

Fig. 29. The measurement results of the PSPR method [42].

6. Conclusion

In this chapter, we reviewed some recent development or state of the art techniques. It shows that the heterodyne interferometry is a mature technique and can be applied to many different aspects. For example, the diffraction grating heterodyne interferometry (DGHI) provided nanometer resolution for precision positioning which can be integrated with motorized stage. Full-field circular heterodyne interferometry (FFCHI) can be used to investigate the two-dimensional optical properties, such as refractive index and birefrigence of testing sample. For this point of view, the heterodyne interferometry can be a refractometer with high accuracy. To integrate with optical sensor, the heterodyne interferometry can be used to diagnose the concentration of the body fluid such as blood glucose and glycerin or the protein interaction between body-antibody. Therefore, the heterodyne interferometry is a powerful, flexible, integrable, and reliable technique for precision metrology.

7. References

[1] L. C. De Backer, “In-plane displacement measurement by speckle interferometry,” Non-destructive Testing 8, pp. 177-180 (1975).

[2] B. Pan, K. Qian, H. Xie, and Anand Asundi, “Two-dimensional digital image correlation for in-plane displacement and strain measurement: a review,” Measurement Science and Technology 20, pp. 062001 (2009).

[3] S. Nakadate, “Vibration measurement using phase shifting time average holographic interferometry,” Applied Optics 25, pp. 4155-4161 (1986).

[4] G. Pedrini, W. Osten, and M. E. Gusev, “High-speed digital holographic interferometry for vibration measurement,” Applied Optics 45, pp. 3456-3462 (2006).

[5] W. B. Ribbens, “Surface roughness measurement by two wavelength holographic interferometry,” Applied Optics 13, pp. 1085-1088 (1974).

[6] C. J. Tay, M. Thakur, C. Quan, “Grating projection system for surface contour measurement,” Applied Optics 44, pp. 1393-1400 (2005).

[7] Haller, H. A. Huggins, and M. J. Freiser, “On the measurement of indices of refraction of nematic liquid,” Molecular Crystals and Liquid Crystal 16, pp. 53-59 (1972).

[8] W. Lukosz and P. Pliska, “Determination of thickness and refractive index of SiO2 films on silicon wafers using an Abbe refractometer,” Optics Communications 85, pp. 381-384 (1991).

[9] J. A. D. Feijter, J. Benjamins, and F. A. Veer, “Ellipsometry as a tool to study the adsorption behavior of synthetic and biopolymers at the air-water interface,” Biopolymers 17, pp. 1759-1772 (1978).

[10] F. L. McCrackin, E. Passaglia, R. R. Stromberg, and H. L. Steinberg, “Measurement of the thickness and refractive index of very thin films and the optical properties of surfaces by ellipsometry,” Journal of Research of the National Bureau of Standards A. Physics and Chemistry 67A, pp. 363-377 (1963).

[11] B. T. Liu, S. J. Tang, Y. Y. Yu, and S. H. Lin, “High refractive index polymer/inorganic hybrid films containing high TiO2 contents,” Colloids and Surfaces A: Physicochemical and Engineering Aspects 377, pp. 138-143 (2011).

[12] C. M. Jan, Y. H. Lee, K. C. Wu, and C. K. Lee, “Integrating fault tolerance algorithm and circularly polarized ellipsometer for point of care applications,” Optics Express 19, pp. 5431-5441 (2011).

[13] H. G. Tompkins and E. A. Irene, *Handbook of Ellipsometry*, Willian Andrew, New York, 2010

[14] R. M. A. Azzam and N. M. Bashara, *Ellipsometry and Polarized Light*, Elsevier Science Publisher, Netherlands, 1992

[15] J. A. Dahlquist, D. G. Peterson, and W. Culshaw, “Zeeman laser interferometer,” Applied Physics Letters 9, pp. 181-183 (1966).

[16] T. Suzuki and R. Hioki, “Translation of light frequency by a moving grating,” Journal of the Optical Society of America 57, pp. 1551 (1967).

[17] W. H. Stevenson, “Optical frequency shifting by means of a rotating diffraction grating,” Applied Optics 9, pp. 649-652 (1970).

[18] M. J. Ehrlich, L. C. Phillips, and J. W. Wagner, “Voltage-controlled acousto-optic phase shifter,” Review of Scientific instrument 59, pp. 2390-2392 (1988).

[19] T. Q. Banh, Y. Ohkubo, Y. Murai, and M. Aketagawa, “Active suppression of air refractive index fluctuation using a Fabry-Perot cavity and a piezoelectric volume actuator,” Applied Optics 50, pp. 53-60 (2011).

[20] D. C. Su, M. H. Chiu, and C. D. Chen, "A heterodyne interferometer using an electro-optic modulator for measuring small displacement," Journal of Optics 27, pp. 19-23 (1996).

[21] W. K. Kuo, J. Y. Kuo, and C. Y. Huang, "Electro-optic heterodyne interferometer," Applied Optics 46, pp. 3144-3149 (2007).

[22] H. Kikuta, K. Iwata, and R. Nagata, "Distance measurement by the wavelength shift of laser diode light," Applied Optics 25, pp. 2976-2980 (1986).

[23] M. Born and E. Wolf, *Principles of Optics*, Cambridge University Press, UK, 1999.

[24] C. K. Lee, C. C. Wu, S. J. Chen, L. B. Yu, Y. C. Chang, Y. F. Wang, J. Y. Chen, and W. J. Wu, "Design and construction of linear laser encoders that possess high tolerance of mechanical runout," Applied Optics 43, pp. 5754-5762 (2004).

[25] C. H. Liu, W. Y. Jywe, and C. K. Chen, "Development of a diffraction type optical triangulation sensor," Applied optics 43, 5607-5613 (2004).

[26] C. F. Kao, C. C. Chang, and M. H. Lu, "Double-diffraction planar encoder by conjugate optics," Optical Engineering 44, pp. 023603-1 (2005).

[27] J. Y. Lee, H. Y. Chen, C. C. Hsu and C. C. Wu, "Optical heterodyne grating interferometry for displacement measurement with subnanometric resolution," Sensors and Actuators A: Physical 137 pp. 185-191 (2007).

[28] C. C. Hsu, C. C. Wu, J. Y. Lee, H. Y. Chen, and H. F. Weng, "Reflection type heterodyne grating interferometry for in-plane displacement measurement," Optics Commun. 281 pp. 2583-2589 (2008).

[29] C. C. Wu, C. C. Hsu, J. Y. Lee, and C. L. Dai, "Optical heterodyne laser encoder with Sub-nanometer resolution," Measurement Science and Technology 19 pp. 045305-045313 (2008).

[30] H. L. Hsieh, J. C. Chen, G. Lerondel, and J. Y. Lee, "Two-dimensional displacement measurement by quasi-common-optical path heterodyne grating interferometer," Optics Express 19, pp. 9770-9782 (2011).

[31] Y. L. Lo and P. F. Hsu, "Birefringence measurements by an electro-optic modulator using a new heterodyne scheme," Optical engineering 41, pp. 2764-2767 (2002).

[32] C. C. Hsu, K. H. Chen, and D. C. Su, "Normal incidence refractometer", Optics Communications 218, pp. 205-211 (2003).

[33] K. H. Chen, C. C. Hsu, and D. C. Su, "A method for measuring the complex refractive index and thickness of a thin metal film," Applied Physics B 77, pp.839-842 (2003).

[34] C. C. Hsu, J. Y. Lee, and D. C. Su, "Thickness and optical constants measurement of thin film growth with circular heterodyne interferometry", Thin Solid Film 491, pp. 91-95 (2005).

[35] C. Y. Hong, J. J. Chieh, S. Y. Yang, H. C. Yang, and H. E. Horng, "Simultaneous identification of the low field induced tiny variation of complex refractive index for anisotropic and opaque magnetic fluid thin film by a stable heterodyne Mach-Zehnder interferometer," Applied Optics 48, pp. 5604-5611 (2009).

[36] J. Y. Lin, "Determination of the refractive index and the chiral parameter of a chiral solution based on chiral reflection equations and heterodyne interferometry," Applied Optics 47, pp. 3828-3834 (2008).

[37] C. C. Hsu and D. C. Su, "Method for determining the optic axis and (ne, no) of a birefringent crystal", Applied Optics 41, pp. 3936-3940, (2002).

[38] Y. L. Chen, H. C. Hsieh, W. T. Wu, W. Y. Chang, and D. C. Su, "Alternative method for measuring the full field refractive index of a gradient index lens with normal incidence heterodyne interferometry," Applied Optics 49, pp. 6888-6892 (2010).
[39] Y. C. Huang, C. Chou, and M. Chang, "Direct measurement of refractive indices of a linear birefringent retardation plate," Optics Communications 133, pp. 11-16 (1997).
[40] J. F. Lin, C. C. Chang, C. D. Syu, Y. L. Lo, and S. Y. Lee, "A new electro-optic modulated circular heterodyne interferometer for measuring the rotation angle in a chiral medium," Optics and Laser in Engineering 47, pp. 39-44 (2009).
[41] M. H. Chiu, S. F. Wang, and R. S. Chang, "D-type fiber biosensor based on surface Plasmon resonance technology and heterodyne interferometry," Optics Letters 30, pp. 233-235 (2005).
[42] C. Chou, H. T. Wu, Y. C. Huang, Y. L. Chen, and W. C. Kuo, "Characteristics of a paired surface plasma waves biosensor," Optics Express 14, pp. 4307-4315 (2006).
[43] J. Y. Lee and S. K. Tsai, "Measurement of refractive index variation of liquids by surface plasmon resonance and wavelength modulated heterodyne interferometry," Optics Communications 284, pp. 925-929 (2011).
[44] T. Q. Lin, Y. L. Lu, and C. C. Hsu, "Fabrication of glucose fiber sensor based on immobilized GOD technique for rapid measurement," Optics Express 18 pp. 27560-27566 (2010).
[45] C. C. Hsu, Y. C. Chen, J.Y. Lee, and C. C. Wu, "Reusable glucose f iber sensor for measuring glucose concentration in serum," Chinese Optics Letters, 9 pp. 100608-1~100608-3 (2011).
[46] J. Y. Lin, J. H. Chen, K. H. Chen, and D. C. Su, "A new type of liquid refractometer," Physics Status Solidi C 5, pp. 1020-1022 (2008).
[47] P. Nath, H. K. Singh, P. Datta, K. C. Sarma, "All fiber optic sensor for measurement of liquid refractive index," Sensors and Actuators A: Physical 148, pp. 16-18 (2008).
[48] Y. L. Yeh, "Real time measurement of glucose concentration and average refractive index using a laser interferometer," Optics and Laser in Engineering 46, pp. 666-670 (2008).
[49] K. S. Kim, Y. Mizuno, M. Nakano, S. Onoda, and K. Nakamura, "Refractive index sensor for liquids and solids using dielectric multilayer films deposited on optical fiber end surface," Photonics Technology Letters 23, pp. 1472-1474 (2011).
[50] H. H. Hamzah, N. A. Yusof, A. B. Salleh, and F. A. Baker, "An optical test strip for the detection of Benzonic acid in food," Sensors 11, pp. 7302-7313 (2011).

Interferometry - Research and Applications in Science and Technology

Edited by Dr Ivan Padron

ISBN 978-953-51-0403-2
Hard cover, 462 pages
Publisher InTech
Published online 21, March, 2012
Published in print edition March, 2012

This book provides the most recent studies on interferometry and its applications in science and technology. It is an outline of theoretical and experimental aspects of interferometry and their applications. The book is divided in two sections. The first one is an overview of different interferometry techniques and their general applications, while the second section is devoted to more specific interferometry applications comprising from interferometry for magnetic fusion plasmas to interferometry in wireless networks. The book is an excellent reference of current interferometry applications in science and technology. It offers the opportunity to increase our knowledge about interferometry and encourage researchers in development of new applications.